Immunohistochemical staining revealed that integrin-β1 had accumulated in the tips of the microglial projections extending toward the periphery of the slices following ADP application. The microglia in slices pretreated with RGD peptides sent out many projections in random directions within 10 min following exposure to ADP, but the microglia retracted the projections and did not continue extending them toward the ADP sources. These observations strongly suggest that interaction between integrin-β1 and the ECM is necessary for microglia to direct their processes and to maintain the elongated processes. Binding of integrin-β1 to ligands is known to promote integrin clustering, activate outside-in signaling pathways, and lead to actin-cytoskeleton reorganization (Berrier and Yamada, 2007). The dot-like staining of integrin-β1 in the tips of microglial processes, as shown in Fig. 6, suggests that the clustered integrin-β1 activates integrin signaling pathways. Activation of the signaling pathways downstream of integrin-β1 may act as positive feedback signals and cooperate with the signaling pathways downstream of $P2Y_{12}$ to regulate directional process extension by microglia.

Most of the microglia on the collagen gel in the process extension assay did not migrate toward ATP within 2 h after ATP stimulation. However, we observed that microglia had migrated into collagen gels toward the ATP after incubation for 4h, and that RGD peptide inhibited the cell migration (data not shown). These observations suggest that integrin-β1 activation is involved in the movement of micoglial cell bodies and that the cell migration requires activation of other signaling pathways in addition to those underlying the process extension. Integrin-β has been reported to be upregulated by activated microglia in pathological states, such as nerve injury or ischemia, (Kang et al., 2008; Kloss et al., 1999). Expression of ECM ligands for integrin-β1 is increased in pathological states, and fibronectin leak to brain parenchyma from blood vessels when blood-brain-barrier is damaged by some pathological conditions (Liesi et al., 1984; Nasu-Tada et al., 2006; Tate et al., 2007). Interactions between integrins and fibronectin have been reported to regulate microglial migration, proliferation, and protein expression (Milner et al., 2007; Nasu-Tada et al., 2005, 2006). The ECM binding to integrins activates intracellular signalings that regulate microglial motility, and therefore may be an important signal for regulating the extent of microglial infiltration at the site of injury and retention there.

In this study, we demonstrated immunohistochemically that the microglia in normal brains express integrin-β1. Most of the integrin-β1 in microglia in the normal brain seems to be inactivated because ECM molecules that bind to integrin-β1 have been reported to be slightly expressed in the normal brain. (Bellail et al., 2004). In the early stage following neuronal injury, ATP may induce integrin-β1 activation in microglia through $P2Y_{12}$. The integrin-β1 activation increases microglial adhesion to the ECM, and that may be an important trigger for process extension by microglia toward the injured region. $P2Y_{12}$-dependent integrin-β1 activation may be crucial for inducing the initial response of microglia to brain damage.

ACKNOWLEDGMENTS

We thank Drs. S. Uchino and T. Namba for advice and discussion.

REFERENCES

Bellail AC, Hunter SB, Brat DJ, Tan C, Van Meir EG. 2004. Microregional extracellular matrix heterogeneity in brain modulates glioma cell invasion. Int J Biochem Cell Biol 36:1046–1069.
Berrier AL, Yamada KM. 2007. Cell-matrix adhesion. J Cell Physiol 213:565–573.
Bo L, Peterson JW, Mork S, Hoffman PA, Gallatin WM, Ransohoff RM, Trapp BD. 1996. Distribution of immunoglobulin superfamily members ICAM-1, -2, -3, and the beta 2 integrin LFA-1 in multiple sclerosis lesions. J Neuropathol Exp Neurol 55:1060–1072.
Burnstock G. 2008. Purinergic signalling and disorders of the central nervous system. Nat Rev Drug Discov 7:575–590.
Cukierman E, Pankov R, Yamada KM. 2002. Cell interactions with three-dimensional matrices. Curr Opin Cell Biol 14:633–639.
Davalos D, Grutzendler J, Yang G, Kim JV, Zuo Y, Jung S, Littman DR, Dustin ML, Gan WB. 2005. ATP mediates rapid microglial response to local brain injury in vivo. Nat Neurosci 8:752–758.
Filtz TM, Li Q, Boyer JL, Nicholas RA, Harden TK. 1994. Expression of a cloned P2Y purinergic receptor that couples to phospholipase C. Mol Pharmacol 46:8–14.
Franke B, Akkerman JW, Bos JL. 1997. Rapid Ca2+-mediated activation of Rap1 in human platelets. EMBO J 16:252–259.
Franke B, van Triest M, de Bruijn KM, van Willigen G, Nieuwenhuis HK, Negrier C, Akkerman JW, Bos JL. 2000. Sequential regulation of the small GTPase Rap1 in human platelets. Mol Cell Biol 20:779–785.
Franke H, Krugel U, Illes P. 2006. P2 receptors and neuronal injury. Pflugers Arch 452:622–644.
Grimpe B, Dong S, Doller C, Temple K, Malouf AT, Silver J. 2002. The critical role of basement membrane-independent laminin gamma 1 chain during axon regeneration in the CNS. J Neurosci 22:3144–3160.
Han J, Lim CJ, Watanabe N, Soriani A, Ratnikov B, Calderwood DA, Puzon-McLaughlin W, Lafuente EM, Boussiotis VA, Shattil SJ, Ginsberg MH. 2006. Reconstructing and deconstructing agonist-induced activation of integrin alphaIIbbeta3. Curr Biol 16:1796–1806.
Haynes SE, Hollopeter G, Yang G, Kurpius D, Dailey ME, Gan WB, Julius D. 2006. The $P2Y_{12}$ receptor regulates microglial activation by extracellular nucleotides. Nat Neurosci 9:1512–1519.
Hirasawa T, Ohsawa K, Imai Y, Ondo Y, Akazawa C, Uchino S, Kohsaka S. 2005. Visualization of microglia in living tissues using Iba1-EGFP transgenic mice. J Neurosci Res 81:357–362.
Honda S, Sasaki Y, Ohsawa K, Imai Y, Nakamura Y, Inoue K, Kohsaka S. 2001. Extracellular ATP or ADP induce chemotaxis of cultured microglia through Gi/o-coupled P2Y receptors. J Neurosci 21:1975–1982.
Hynes RO. 2002. Integrins: Bidirectional, allosteric signaling machines. Cell 110:673–687.
Imai Y, Ibata I, Ito D, Ohsawa K, Kohsaka S. 1996. A novel gene iba1 in the major histocompatibility complex class III region encoding an EF hand protein expressed in a monocytic lineage. Biochem Biophys Res Commun 224:855–862.
Inoue K. 2006. The function of microglia through purinergic receptors: Neuropathic pain and cytokine release. Pharmacol Ther 109:210–226.
Irino Y, Nakamura Y, Inoue K, Kohsaka S, Ohsawa K. 2008. Akt activation is involved in $P2Y_{12}$ receptor-mediated chemotaxis of microglia. J Neurosci Res 86:1511–1519.
Jones LS. 1996. Integrins: Possible functions in the adult CNS. Trends Neurosci 19:68–72.
Jucker M, Kleinman HK, Hohmann CF, Ordy JM, Ingram DK. 1991. Distinct immunoreactivity to 110 kDa laminin-binding protein in adult and lesioned rat forebrain. Brain Res 555:305–312.
Kang WS, Choi JS, Shin YJ, Kim HY, Cha JH, Lee JY, Chun MH, Lee MY. 2008. Differential regulation of osteopontin receptors, CD44 and the alpha(v) and beta(3) integrin subunits, in the rat hippocampus following transient forebrain ischemia. Brain Res 1228:208–216.
Kinashi T. 2005. Intracellular signalling controlling integrin activation in lymphocytes. Nat Rev Immunol 5:546–559.

Kloss CU, Werner A, Klein MA, Shen J, Menuz K, Probst JC, Kreutzberg GW, Raivich G. 1999. Integrin family of cell adhesion molecules in the injured brain: Regulation and cellular localization in the normal and regenerating mouse facial motor nucleus. J Comp Neurol 411:162–178.

Koizumi S, Fujishita K, Tsuda M, Shigemoto-Mogami Y, Inoue K. 2003. Dynamic inhibition of excitatory synaptic transmission by astrocyte-derived ATP in hippocampal cultures. Proc Natl Acad Sci USA 100:11023–11028.

Kreutzberg GW. 1996. Microglia: A sensor for pathological events in the CNS. Trends Neurosci 19:312–318.

Krum JM, More NS, Rosenstein JM. 1991. Brain angiogenesis: Variations in vascular basement membrane glycoprotein immunoreactivity. Exp Neurol 111:152–165.

Kurpius D, Nolley EP, Dailey ME. 2007. Purines induce directed migration and rapid homing of microglia to injured pyramidal neurons in developing hippocampus. Glia 55:873–884.

Kurpius D, Wilson N, Fuller L, Hoffman A, Dailey ME. 2006. Early activation, motility, and homing of neonatal microglia to injured neurons does not require protein synthesis. Glia 54:58–70.

Liesi P. 1990. Extracellular matrix and neuronal movement. Experientia 46:900–907.

Liesi P, Kaakkola S, Dahl D, Vaheri A. 1984. Laminin is induced in astrocytes of adult brain by injury. EMBO J 3:683–686.

Milner R, Campbell IL. 2002a. The integrin family of cell adhesion molecules has multiple functions within the CNS. J Neurosci Res 69:286–291.

Milner R, Campbell IL. 2002b. Cytokines regulate microglial adhesion to laminin and astrocyte extracellular matrix via protein kinase C-dependent activation of the alpha6beta1 integrin. J Neurosci 22:1562–1572.

Milner R, Crocker SJ, Hung S, Wang X, Frausto RF, del Zoppo GJ. 2007. Fibronectin- and vitronectin-induced microglial activation and matrix metalloproteinase-9 expression is mediated by integrins alpha5beta1 and alphavbeta5. J Immunol 178:8158–8167.

Nakajima K, Kohsaka S. 2005. Response of microglia to brain injury. In: Kettenmann H, Ransom B, editors. Neuroglia, 2nd ed. New York: Oxford University Press. pp 443–453.

Nakajima K, Shimojo M, Hamanoue M, Ishiura S, Sugita H, Kohsaka S. 1992. Identification of elastase as a secretory protease from cultured rat microglia. J Neurochem 58:1401–1408.

Nasu-Tada K, Koizumi S, Inoue K. 2005. Involvement of beta1 integrin in microglial chemotaxis and proliferation on fibronectin: Different regulations by ADP through PKA. Glia 52:98–107.

Nasu-Tada K, Koizumi S, Tsuda M, Kunifusa E, Inoue K. 2006. Possible involvement of increase in spinal fibronectin following peripheral nerve injury in upregulation of microglial $P2X_4$, a key molecule for mechanical allodynia. Glia 53:769–775.

Neumann J, Sauerzweig S, Ronicke R, Gunzer F, Dinkel K, Ullrich O, Gunzer M, Reymann KG. 2008. Microglia cells protect neurons by direct engulfment of invading neutrophil granulocytes: A new mechanism of CNS immune privilege. J Neurosci 28:5965–5975.

Nimmerjahn A, Kirchhoff F, Helmchen F. 2005. Resting microglial cells are highly dynamic surveillants of brain parenchyma in vivo. Science 308:1314–1318.

Nolte C, Kirchhoff F, Kettenmann H. 1997. Epidermal growth factor is a motility factor for microglial cells in vitro: Evidence for EGF receptor expression. Eur J Neurosci 9:1690–1698.

Ohsawa K, Irino Y, Nakamura Y, Akazawa C, Inoue K, Kohsaka S. 2007. Involvement of $P2X_4$ and $P2Y_{12}$ receptors in ATP-induced microglial chemotaxis. Glia 55:604–616.

Oinuma I, Katoh H, Negishi M. 2006. Semaphorin 4D/Plexin-B1-mediated R-Ras GAP activity inhibits cell migration by regulating beta(1) integrin activity. J Cell Biol 173:601–613.

Simon J, Filippov AK, Goransson S, Wong YH, Frelin C, Michel AD, Brown DA, Barnard EA. 2002. Characterization and channel coupling of the P2Y(12) nucleotide receptor of brain capillary endothelial cells. J Biol Chem 277:31390–31400.

Tadokoro S, Shattil SJ, Eto K, Tai V, Liddington RC, de Pereda JM, Ginsberg MH, Calderwood DA. 2003. Talin binding to integrin beta tails: A final common step in integrin activation. Science 302:103–106.

Tate CC, Garcia AJ, LaPlaca MC. 2007. Plasma fibronectin is neuroprotective following traumatic brain injury. Exp Neurol 207:13–22.

Tsuda M, Shigemoto-Mogami Y, Koizumi S, Mizokoshi A, Kohsaka S, Salter MW, Inoue K. 2003. $P2X_4$ receptors induced in spinal microglia gate tactile allodynia after nerve injury. Nature 424:778–783.

Webb SE, Pollard JW, Jones GE. 1996. Direct observation and quantification of macrophage chemoattraction to the growth factor CSF-1. J Cell Sci 109 (Pt 4):793–803.

Wu LJ, Vadakkan KI, Zhuo M. 2007. ATP-induced chemotaxis of microglial processes requires P2Y receptor-activated initiation of outward potassium currents. Glia 55:810–821.

Zhou FC. 1990. Four patterns of laminin-immunoreactive structure in developing rat brain. Brain Res Dev Brain Res 55:191–201.

Neuroscience 167 (2010) 372–383

PIGMENT EPITHELIUM-DERIVED FACTOR UP-REGULATION INDUCED BY MEMANTINE, AN N-METHYL-D-ASPARTATE RECEPTOR ANTAGONIST, IS INVOLVED IN INCREASED PROLIFERATION OF HIPPOCAMPAL PROGENITOR CELLS

T. NAMBA,[a1] T. YABE,[b] Y. GONDA,[a] N. ICHIKAWA,[c] T. SANAGI,[a] E. ARIKAWA-HIRASAWA,[c] H. MOCHIZUKI,[d] S. KOHSAKA[a*] AND S. UCHINO[a]

[a]*Department of Neurochemistry, National Institute of Neuroscience, Tokyo 187-8502, Japan*

[b]*Kitasato Institute for Life Sciences, Kitasato University, Tokyo 108-8641, Japan*

[c]*Research Institute for Diseases of Old Age, Juntendo University School of Medicine, Tokyo 113-8431, Japan*

[d]*Department of Neurology, Kitasato University, Kanagawa 228-8555, Japan*

Abstract—Memantine is classified as an NMDA receptor antagonist. We recently reported that memantine promoted the proliferation of neural progenitor cells and the production of mature granule neurons in the adult hippocampus. However, the molecular mechanism responsible for the memantine-induced promotion of cellular proliferation remains unknown. In this study we searched for a factor that mediates memantine-induced cellular proliferation, and found that pigment epithelium-derived factor (PEDF), a broad-acting neurotrophic factor, is up-regulated in the dentate gyrus of adult mice after the injection of memantine. PEDF mRNA expression increased significantly by 3.5-fold at 1 day after the injection of memantine. In addition, the expression level of PEDF protein also increased by 1.8-fold at 2 days after the injection of memantine. Immunohistochemical study using anti-PEDF antibody showed that the majority of the PEDF-expressing cells were protoplasmic and perivascular astrocytes. Using a neurosphere assay, we confirmed that PEDF enhanced cellular proliferation under the presence of fibroblast growth factor-2 (FGF-2) and epidermal growth factor (EGF) but was not involved in the multilineage potency of hippocampal progenitor cells. Over expression of PEDF by adeno-associated virus, however, did not stimulate cellular proliferation, suggesting PEDF *per se* does not promote cellular proliferation *in vivo*. These findings suggest that the memantine induced PEDF up-regulation is involved in increased proliferation of hippocampal progenitor cells.

Key words: neurogenesis, hippocampus, PEDF, NMDA receptor, memantine.

Neurogenesis persists throughout life in the hippocampi of mammals, including humans (Altman and Das, 1965; Seki and Arai, 1993; Eriksson et al., 1998; Ming and Song, 2005; Namba et al., 2005). Neural progenitor cells divide and give rise to new neurons in at least two regions of the adult brain: the dentate gyrus (DG) of the hippocampus and the subventricular zone (SVZ) of the lateral ventricle (Alvarez-Buylla et al., 2002; Ming and Song, 2005). We recently demonstrated that memantine, an uncompetitive N-methyl-D-aspartate (NMDA) receptor antagonist that is used clinically for the treatment of Alzheimer's disease, increased the proliferation of progenitor cells and promoted the subsequent production of new neurons in adult hippocampus (Maekawa et al., 2009; Namba et al., 2009). However, the molecular mechanism responsible for the memantine-induced promotion of cellular proliferation remains unclear. Since recent electrophysiological studies have shown that progenitor cells in adult hippocampus fail to respond to NMDA (Tozuka et al., 2005), functional NMDA receptors are probably not expressed in progenitor cells (Petrus et al., 2009). Therefore, indirect mechanisms might underlie the effect of memantine on the proliferation of progenitor cells. Previous studies have demonstrated that brain-derived neurotrophic factor (BDNF) and fibroblast growth factor-2 (FGF-2) are up-regulated by treatment with memantine (Marvanova et al., 2001; Namba et al., 2009). However, no evidence suggesting that BDNF and FGF-2 stimulate the proliferation of hippocampal progenitor cells has been obtained (Kuhn et al., 1997; Wagner et al., 1999; Sairanen et al., 2005), although BDNF has been shown to influence the survival of newly generated cells (Sairanen et al., 2005). In the present study, we found that pigment epithelium-derived factor (PEDF), in addition to BDNF and FGF-2, was up-regulated by treatment with memantine.

PEDF is a 50-kDa glycoprotein and a non-inhibitory member of the serine protease inhibitor gene family (Tombran-Tink and Barnstable, 2003). Its biological activity was first identified in a conditioned medium of cultured human fetal retinal pigment epithelial cells, which induced the neuronal differentiation of cultured human Y-79 retinoblastoma cells (Tombran-Tink et al., 1991). PEDF is expressed in various regions of the brain, including neuronal and glial cells, and has neurotrophic and neuroprotective effects in

[1] Present address: Department of Cell Pharmacology, Nagoya University Graduate School of Medicine, Nagoya 466-8550, Japan.

*Corresponding author. Tel: +81-42-346-1711; fax: +81-42-346-1741.
E-mail address: kohsaka@ncnp.gp.jp (S. Kohsaka).

Abbreviations: AAV, adeno-associated virus; AD, Alzheimer's disease; BDNF, brain-derived neurotrophic factor; BrdU, 5-bromo-2-deoxyuridine; BSA, bovine serum albumin; DG, dentate gyrus; FGF-2, fibroblast growth factor-2; GAPDH, glyceraldehydes-3-phosphate dehydrogenase; GCL, granule cell layer; GFAP, glial fibrillary acidic protein; NMDA, N-methyl-D-aspartate; PEDF, pigment epithelium-derived factor; PFA, paraformaldehyde; RT-PCR, reverse transcription-PCR; SVZ, subventricular zone.

0306-4522/10 $ - see front matter © 2010 IBRO. Published by Elsevier Ltd. All rights reserved.
doi:10.1016/j.neuroscience.2010.01.033

various types of neurons (Tombran-Tink and Barnstable, 2003; Yabe et al., 2005; Sanagi et al., 2007). Interestingly, Ramirez-Castillejo et al. (2006) showed that PEDF was secreted from ependymal and endothelial cells of adult SVZ and promoted the self-renewal of adult neural stem cells in the SVZ; these results indicated that PEDF plays a role in the maintenance of neural stem cells, functioning as a niche-derived regulator in the SVZ (Ramirez-Castillejo et al., 2006). In the present study, we provide novel findings showing that the expression of PEDF was increased by treatment with memantine and that PEDF promoted the proliferation of hippocampal progenitor cells, suggesting that PEDF is an intriguing factor involved in the memantine-induced promotion of cellular proliferation in adult hippocampus.

EXPERIMENTAL PROCEDURES

The animals used in this study were 3-month-old male and postnatal day 1 (P1) C57BL6/J mice (Clea Japan Inc., Tokyo, Japan). All experimental procedures were approved by The Animal Care and Use Committee of the National Institute of Neuroscience.

Animals and drug administration

Mice were injected i.p. with memantine (Sigma, St. Louis, MO, USA) at a dose of 10, 30, or 50 mg/kg body weight. Control mice were injected i.p. with the same volume of 0.9% saline (Ohtsuka Pharmaceuticals, Tokyo, Japan). After 1, 2, or 3 days, the mice were injected i.p. with 75 mg/kg body weight of 5-bromo-2-deoxyuridine (BrdU; Sigma) three times at intervals of 2 h. The mice were then sacrificed at 1 day after BrdU-injection.

Tissue preparation

After the mice were deeply anesthetized with sodium pentobarbital (Kyoritsu Pharmaceuticals, Tokyo, Japan), the mice were transcardially perfused with 4% paraformaldehyde (PFA) in 0.1 M phosphate-buffered saline (PBS). The brains were then removed and immersion-fixed at 4 °C overnight in the same fixative. After washing in PBS, the brains were successively equilibrated in 10 and 20% sucrose in PBS, embedded in Tissue-Tek optimal cutting temperature compound (Sakura, Tokyo, Japan), and frozen in liquid nitrogen (Seki et al., 2007).

Immunohistochemistry

For immunostaining with anti-BrdU antibody, frozen brains were coronally sliced into 14-μm sections using a cryostat (CM-3000; Leica, Nussloch, Germany) and mounted on an MAS-coated glass slide (SUPERFROST; Matsunami, Osaka). The sections were boiled in 0.01 M citrate buffer for 15 min, incubated in 2N HCl at 37 °C for 35 min, and washed in PBS. The sections were then incubated with rat monoclonal anti-BrdU antibody (1:400; Morpho-Sys UK Ltd., Oxford, UK) at 4 °C overnight in PBS containing 1% bovine serum albumin (BSA). After washing in PBS, they were then incubated at room temperature for 1–2 h in PBS containing 1% BSA plus Cy3-conjugated anti-rat IgG antibody (1:200; Jackson, West Grove, PA, USA). For immunostaining with other antibodies, immunohistochemistry was performed using a floating method as described previously (Namba et al., 2009). Briefly, the frozen brains were coronally sliced into 40-μm sections using a cryostat (CM-3000). After washing in PBS, the sections were incubated at 4 °C overnight with rabbit polyclonal anti-PEDF antibody (1:400; Sanagi et al. (2007)) and mouse monoclonal anti-glial fibrillary acidic protein (GFAP) antibody (1:1000; Sigma), then incubated at room temperature for 1–2 h with Cy2-conjugated anti-mouse IgG (1:200; Jackson), and Cy3-conjugated anti-rabbit IgG antibody (1:200; Jackson). For endothelial cell detection, the sections were labeled with Alexa Fluor 488-conjugated lectin B4 (IB4; Invitrogen, Carlsbad, CA, USA). After washing in PBS, the sections were mounted on an MAS-coated glass slide and examined for fluorescent signals using a confocal laser-scanning microscope (FV1000; Olympus, Tokyo, Japan). BrdU-labeled cells throughout the rostro-caudal extent of the DG were counted in every sixth section, and the total number of BrdU-labeled cells was calculated by multiplying the count (Maekawa et al., 2005).

Reverse transcription-PCR (RT-PCR)

Total RNA was extracted from the dissected DG or neurospheres prepared from P1 hippocampus using an RNeasy Plus Mini kit (QIAGEN, Germantown, ML, USA), and cDNA was synthesized using an Advantage RT-for-PCR kit (Clontech, Palo Alto, CA, USA) according to the manufacturer's instructions. PCR was performed using Ex Taq (Takara, Shiga, Japan) and a thermal cycler (Verti; Applied Biosystems, Foster City, CA, USA). The primers, annealing temperatures, and sizes of the PCR products are shown in Table 1. The thermocycle conditions were as follows: 30 s at 98 °C, 50 s at the annealing temperature (Table 1), 40 s at 72 °C for 30 cycles (BDNF, FGF-2, VEGF and PEDF), and 45 cycles (EGF) or 25 cycles (glyceraldehydes-3-phosphate dehydrogenase (GAPDH), which was used as an internal control).

A real-time PCR analysis was performed using the SYBER green labeling system (SYBER Premix Ex Taq 2; Takara) and the ABI Prism 7700 Sequence Detection System (Applied Biosystems). Amplifications were carried out in a 96-well optical plate, and the thermocycle conditions were as follows: 5 s at 95 °C, 10 s at 55 °C, and 30 s at 72 °C for 40 cycles. A quantitative analysis was performed using the delta-delta Ct method with GAPDH as an internal control (Kodomari et al., 2009).

Immunoblot analysis

Cell lysate was prepared from the dissected DG at 2 days after the injection of memantine or saline, as described previously (Hattori et al., 2006). Briefly, the dissected DG was homogenized in lysis buffer (10 mM Tris–HCl (pH 7.5), 150 mM NaCl, 1 mM EDTA, 1% Triton X-100, 0.1% sodium deoxycholate, 0.1% SDS, and protease inhibitor cocktail (Roche Diagnostics, Mannheim, Germany)

Table 1. Primer sequences for PCR

Name	Forward primer (5′–3′)	Reverse primer (5′–3′)	Condition (°C)	Amplification size (bp)	Accession No.
BDNF	GGACTCTGGAGAGCGTGAAT	GTCCTCATCCAGCAGCTCTT	55	107	NM_007540
EGF	AGAGCCAGTTCAGTAGAAACTGGG	ACTTTGGTTTCTAATGATTTTCTCC	55	256	NM_010113
FGF-2	AACCGGTACCTTGCTATGAAG	GTTCGTTTCAGTGCCACATAC	55	152	NM_008006
GAPDH	GTCATCATCTCCGCCCCTTCTGC	GATGCCTGCTTCACCACCTTCTTG	55	443	NM_008084
PEDF	GGCAGTGGGTAACCAAGTTTG	GCAGCTGGGCAATCTTGCAG	55	156	NM_011340
VEGF	GACACACCCACCCACATACA	AAAGGACTTCGGCCTCTCTC	60	247	NM_001025250

using a Polytoron homogenizer. After removing the insoluble material by centrifugation (2000×*g*, 4 °C, 10 min), the protein concentration in the supernatant was determined using BCA protein assay reagent (Pierce, Rockford, IL, USA).

The proteins were separated by electrophoresis using an SDS polyacrylamide gel (SuperSep 15–20%; Wako Pure Chemical Industries, Osaka, Japan) and then electrophoretically transferred to a nitrocellulose membrane (Immobilon; Millipore, Bedford, MA, USA). The membrane was blocked by incubation at room temperature for 1 h with 5% skim milk in Tris-buffered saline containing 0.1% Tween 20 (TBST) and then incubated at 4 °C overnight with mouse monoclonal anti-human PEDF antibody (1:500; Trans Genic Inc., Hyogo, Japan). After washing in TBST, the membrane was incubated with horseradish peroxidase-conjugated anti-rabbit IgG secondary antibody (1:1000; Sigma) at room temperature for 1 h. Immunoreactive bands were visualized using a chemiluminescence detection system (ECL; Amersham Biosciences, Piscataway, NJ, USA). The membrane was then incubated with Stripping buffer (62.5 mM Tris–HCl (pH 7.5), 2% SDS, 100 mM 2-mercaptoethanol) at 60 °C for 30 min, blocked with 3% skim milk in TBST, re-probed with anti-β actin antibody (1:1000; Sigma), and then incubated with horseradish peroxidase-conjugated anti-rabbit IgG secondary antibody (1:1000; Sigma). The density of the bands was measured using NIH ImageJ software. Each sample was normalized with the density of the β-actin signal.

Preparation of neurospheres and immunocytochemistry

Neurospheres were prepared from the hippocampus of P1 mouse as described previously (Walker et al., 2008). Briefly, the hippocampus was dissected, filtered through Cell Strainer (BD Falcon 40 μm; BD Biosciences, Bedford, MA, USA), and centrifuged at 1000 rpm for 5 min. The pellet was suspended in neurosphere growth medium (mouse NeuroCult NSC Basal Medium plus mouse NeuroCult NSC Proliferation Supplements) (Stem Cell Technologies, Vancouver, BC, Canada) with 2 μg/ml heparin (Sigma), 20 ng/ml purified mouse receptor grade EGF (Roche Diagnostics) and 10 ng/ml recombinant bovine FGF-2 (Roche Diagnostics). The cells were plated at a density of 2×10^4 cells/ml in a 12-well plate (Corning, Corning, NY, USA) and incubated at 37 °C under an atmosphere of humidified 5% CO_2 for the indicated periods. Recombinant human PEDF was prepared from *Escherichia coli* expressing human PEDF as described previously (Yabe et al., 2005) and added to the growth medium of neurospheres at a concentration of 25 ng/ml. To generate secondary neurospheres, primary neurospheres at DIV7 were harvested, dissociated and then plated at a density of 2×10^4 cells/ml in a 12-well plate (Corning). The cells were incubated for 5 days in neurosphere growth medium with heparin, EGF and FGF-2 but without PEDF.

For the cellular proliferation assay, the neurospheres were cultured for 4 days in neurosphere growth medium, incubated in the presence or in the absence of 25 ng/ml PEDF for 12 h and subsequently maintained with 1 μM BrdU for 2 h. The neurospheres were then dissociated and collected by centrifugation (900 rpm, 5 min). The pellet was suspended in 4% PFA for 5 min and the cells were mounted onto an MAS-coated glass slide. The cells were washed with PBS and incubated in 2N HCl at 37 °C for 35 min. After washing in PBS, they were incubated with anti-BrdU antibody (1:400) at 4 °C for 1 h in PBS containing 1% BSA and 0.1% Triton X-100. After washing in PBS, they were then incubated at room temperature for 1–2 h in PBS containing 1% BSA plus Cy3-conjugated anti-rat IgG antibody (1:200) and Hoechst, and examined for fluorescent signals using a fluorescence microscope (AX70; Olympus, Tokyo, Japan). To examine the cellular proliferation using an anti-phosphorylated histone H3 antibody, the neurospheres were immunostained with mouse monoclonal anti-phosphorylated histone H3 antibody (1:200; Cell Signaling Technology, Danvers, MA, USA) and Cy3-conjugated anti-mouse IgG antibody (1:200) according to the immunocytochemical method described above.

For the cell differentiation assay, the neurospheres were plated onto poly-L-lysine-coated coverslips in NeuroCult NSC Basal Medium containing mouse NeuroCult NSC Proliferation Supplements and 2% fetal calf serum without EGF and FGF-2 and were cultured for 5 days. The differentiated cells were incubated with mouse monoclonal anti-O4 antibody (1:100, Chemicon) at 37 °C for 1 h, washed with PBS, and then fixed with 4% PFA at room temperature for 10 min. After washing in PBS, they were incubated with rabbit polyclonal anti-GFAP antibody (1:800; Dako, Glostrup, Denmark) and goat polyclonal anti-doublecortin (Dcx) antibody (1:400; Santa Cruz Biotechnology, Santa Cruz, CA, USA) at 4 °C for 1 h in PBS containing 1% BSA and 0.1% Triton X-100. After washing in PBS, the cells were then incubated at room temperature for 1–2 h in PBS containing 1% BSA plus Cy5-conjugated anti-rabbit IgG antibody (1:200), Cy3-conjugated anti-goat IgG antibody (1:200), and Cy2-conjugated anti-mouse IgM antibody (1:200). The fluorescent signals were examined using a confocal laser-scanning microscope (FV1000).

Infection of adeno-associated virus (AAV) into dentate gyrus *in vivo*

AAV carrying mouse PEDF cDNA (mPEDF) was prepared according to the manufacturer's instructions. Briefly, FLAG-tagged mPEDF cDNA (Hosomichi et al., 2005) was cloned into the plasmid pAAVMCS under CMV promoter (Stratagene, La Jolla, CA, USA) (pAAVMCS-mPEDF). HEK293 cells were transfected with pAAVMCS-mPEDF or pAAVMCS-EGFP (Yasuda et al., 2007) using Lipofectamine 2000 reagent (Invitrogen). The cells were harvested at 48 h after the transfection, and then AAV was purified by ultracentrifugation (13,000×*g*, 4 °C, 18.5 h). To confirm the expression of mPEDF, COS7 cells were infected with AAV-mPEDF or AAV-EGFP. The cultured medium was collected 48 h after the infection, and then the expression of mPEDF was checked by immunoblotting using mouse monoclonal anti-FLAG antibody (1:1000; Sigma) (Fig. 7A). The AAV-mPEDF and AAV-EGFP (0.95+0.05 μl/injection) or the AAV-EGFP (1 μl/injection) as a control was stereotaxically injected into the DG (anteroposterior, 2.5 mm; lateral, 2.0 mm; ventral, 3.0 mm from bregma, respectively) as described previously (Seki et al., 2007).

Statistical analysis

Data were evaluated using a one-way analysis of variance followed by a post-hoc Scheffé *F*-test. All values were expressed as the mean±SEM, and *P*-values less than 0.05 were considered significant.

RESULTS

Memantine increases cellular proliferation in adult hippocampus

To investigate the effect of memantine on cellular proliferation in adult hippocampus, we injected the mice with a dose of 10, 30, and 50 mg/kg of memantine followed by the injection of BrdU 3 days thereafter. The brains were then fixed 1 day later; after preparing the brain sections, we immunostained them with anti-BrdU antibody, and then counted the number of BrdU-labeled cells. The number of BrdU-labeled cells was significantly increased at a dose of 50 mg/kg of memantine (Fig. 1A; control: 3476.0±149.9 cells/DG, n=4, 10 mg/kg: 3204.0±210.9 cells/DG, n=4, 30 mg/kg: 3137.0±137.2 cells/DG, n=4, 50 mg/kg: 8103.0±

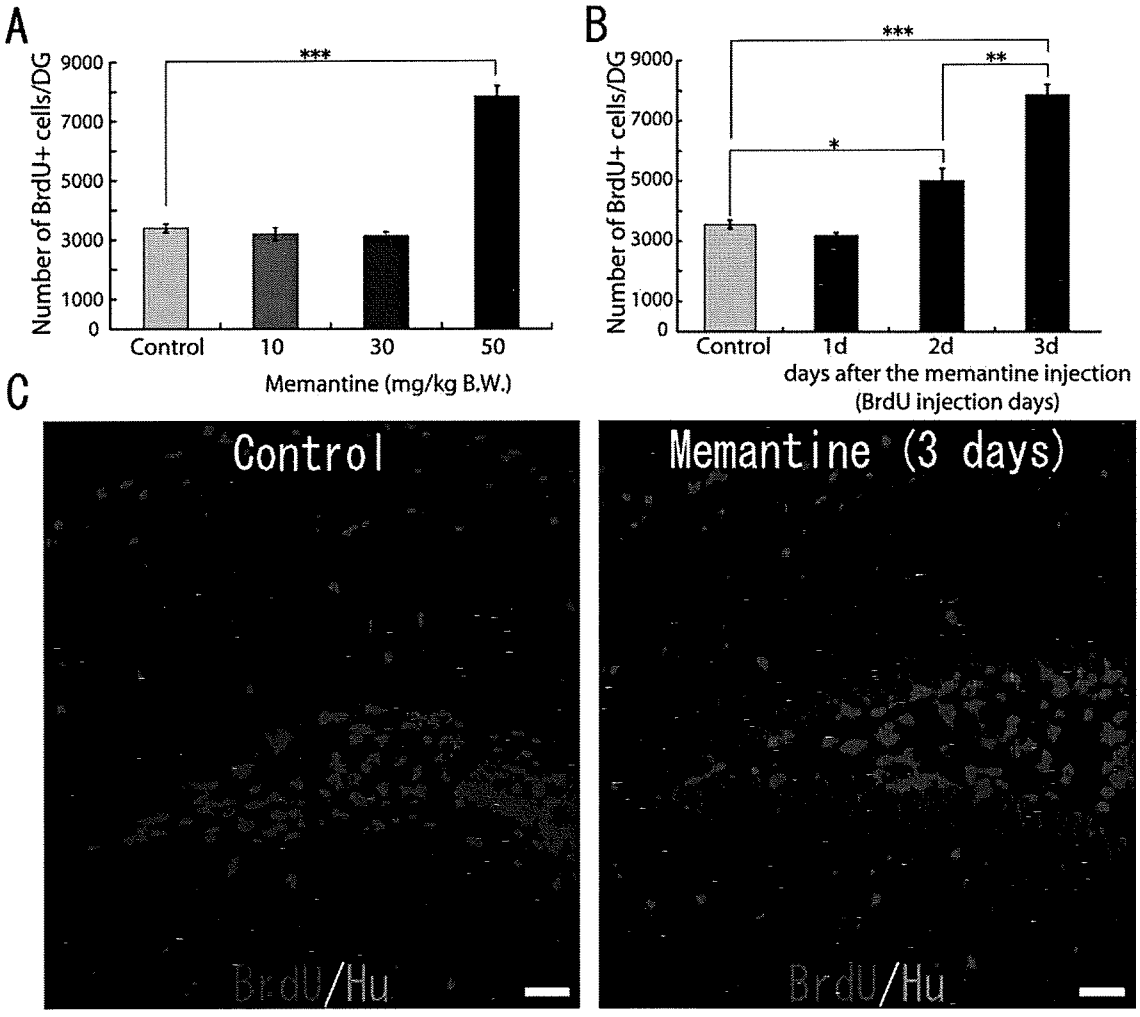

Fig. 1. Effect of memantine on cellular proliferation in the GCL. (A) Dose effect of memantine on cellular proliferation in the GCL. Three-month-old mice were injected i.p. with a dose of 10, 30, 50 mg/kg memantine and injected i.p. with BrdU one day after the memantine-injection. The brains were fixed 3 days after the BrdU-injection, stained with anti-BrdU antibody and the BrdU-labeled cells were counted. *** $P<0.000\,001$. (B) Temporal effect of memantine on cellular proliferation in the GCL. Three-month-old mice were injected i.p. with a dose of 50 mg/kg memantine and injected i.p. with BrdU 1, 2, or 3 days after the memantine-injection. The brains were fixed one day after BrdU-injection, stained with anti-BrdU antibody and the BrdU-labeled cells were counted. * $P<0.05$, ** $P<0.001$, *** $P<0.000\,001$. Error bars indicate standard error of the mean. (C) Representative examples of BrdU-labeled cells (red) in the control group (left panel) and the memantine-injected group (right panel). The sections were co-stained with Hoechst (blue). Scale bars=50 μm.

321.6 cells/DG, $n=4$). Next, to investigate the temporal effect of memantine, we injected the mice with a dose of 50 mg/kg of memantine followed by the injection of BrdU 1, 2 or 3 days thereafter. The brains were then fixed 1 day after each BrdU-injection; after preparing the brain sections, we immunostained them with anti-BrdU antibody, and then counted the number of BrdU-labeled cells. The number of BrdU-labeled cells gradually increased after the injection of memantine (Fig. 1B, C; control: 3393.6±142.4 cells/DG, $n=5$, 1 day after memantine-injection: 3160.0±122.7 cells/DG, $n=3$, 2 days after memantine-injection: 5001.3±420.7 cells/DG, $n=3$, 3 days after memantine-injection: 7851.2±354.2 cells/DG, $n=5$). These results indicate that memantine increases cellular proliferation in adult hippocampus.

To examine whether the memantine directly affects proliferation of progenitor cells using neurospheres prepared from neonatal mouse hippocampus, we initially confirmed that memantine-treatment increased the number of BrdU-labeled cells in the neonatal hippocampus *in vivo* as well as in the adult hippocampus (Fig. 2B, C; control: 12504.0±874.0 cells/DG, $n=3$, 50 mg/kg: 16876.0±499.4 cells/DG, $n=3$, $P<0.05$). Neurospheres were cultured for 7 days in the presence or in the absence (control) of 1 μM memantine, and the numbers of the large size of primary neurospheres (more than 100 μm in diameter) and the small size of neurospheres were counted (Fig. 2D, E; memantine: 44.2±3.2 large size of neurospheres/well and 132.2±13.4 small size of neurospheres/well, $n=5$, control: 48.8±3.5 large size of neurospheres/well and 137.4±13.7 small size of neurospheres/well, $n=5$). These results indicate that these are no significant differences in the number of both sizes of neurospheres in between memantine-treated and untreated cultures, suggesting that memantine fails to affect directly proliferation of the hippocampal progenitor cells.

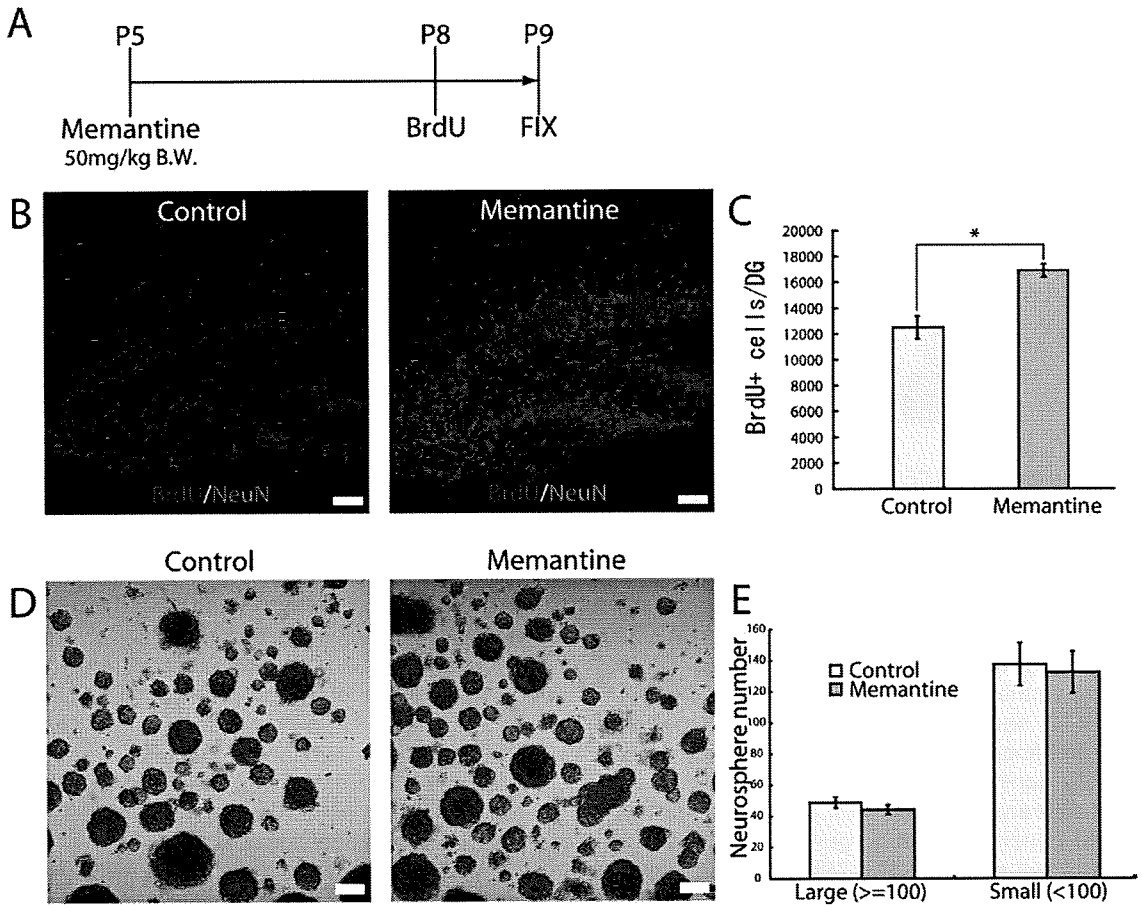

Fig. 2. Effect of memantine on cellular proliferation of hippocampal progenitor cells *in vivo* and *in vitro*. (A) Schematic illustration of the *in vivo* experimental design. (B) Representative examples of BrdU-labeled cells (red) in the DG. P5 mice were injected i.p. with a dose of 50 mg/kg memantine, and with BrdU 3 days after the memantine-injection. The brains were fixed one day after the BrdU-injection and stained with anti-BrdU antibody. The sections were co-stained with Hoechst (blue). (C) Quantitative analysis of the number of BrdU-positive cells in the DG. * $P<0.05$. (D) Primary neurosphere formation. Neurospheres prepared from P1 mouse hippocampus were cultured for 7 days in the absence (control) or in the presence of 1 μM memantine. (E) Quantitative analysis of the number of neurospheres. Scale bars=50 μm in panel B and 100 μm in panel D. Error bars indicate standard deviation.

Memantine up-regulates PEDF expression in adult hippocampus

To search for a factor that mediates the memantine-induced increase in cellular proliferation, we used RT-PCR to investigate gene expression in the DG of memantine-injected mice (50 mg/kg i.p.) and saline-injected (control) mice 1 day after the injection of memantine or saline. We found that the expressions of BDNF, FGF-2 and PEDF were clearly increased after the injection of memantine, whereas the expression levels of EGF and VEGF were not significantly changed (Fig. 3A). Since previous studies showed that neither BDNF nor FGF-2 stimulated the cell proliferation of neural progenitor cells in adult hippocampus (Kuhn et al., 1997; Walker et al., 2008), we here examined the effect of memantine on the expression of PEDF by using real-time PCR technique. The expression of PEDF mRNA was significantly increased 1, 2 and 3 days after memantine-injection (1 day: 3.46-fold, $P=0.0014$, 2 days: 3.51-fold, $P=0.0022$, 3 days: 2.66-fold, $P=0.040$, $n=3$ animals per each group) (Fig. 3B). The expression level of PEDF protein was also increased by 1.79-fold ($n=3$) 2 days after the injection of memantine (Fig. 4A, B). An immnohistochemical study using anti-PEDF antibody showed the prominent expression of PEDF in the hippocampal fissure, the molecular layer, hilus and subgranular zone (SGZ) of the DG (Fig. 4C–F). These results indicate that memantine up-regulates PEDF expression in the DG. In addition, most of the cells expressing PEDF in the molecular layer were positive for anti-GFAP antibody, suggesting that the majority of the PEDF-expressing cells were protoplasmic astrocytes (Fig. 4D) and perivascular astrocytes (Fig. 4E).

PEDF stimulates cellular proliferation of hippocampal progenitor cells *in vitro*

We next investigated the effect of PEDF on cellular proliferation using a neurosphere assay. When neurospheres prepared from P1 mouse hippocampus were cultured for 7 days in the absence (control) or presence of PEDF (25 ng/ml) together with EGF and FGF-2, the number of large

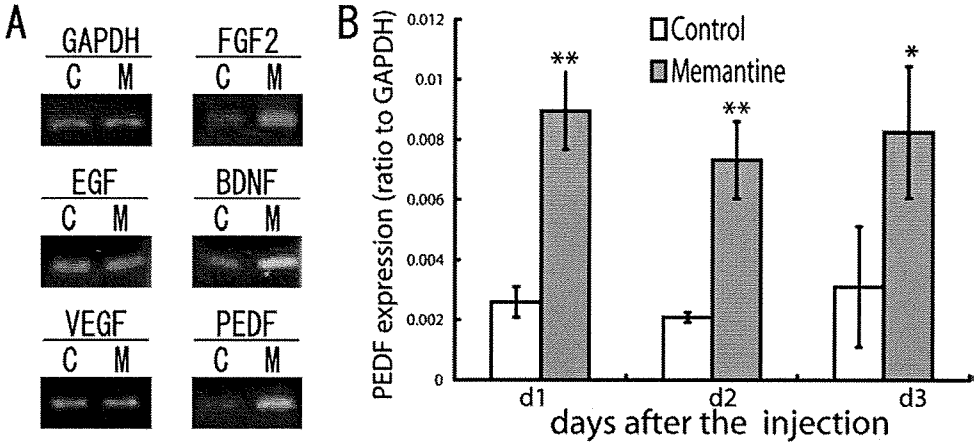

Fig. 3. Increased expression of PEDF mRNA in the DG after the injection of memantine. (A) RT-PCR analysis. Total RNA was prepared from the dissected DG of saline-injected mice (C; control) or mice injected with 50 mg/kg of memantine (M). (B) Temporal analysis of PEDF mRNA expression. The ratio of PEDF mRNA expression (PEDF/GAPDH) was evaluated using a real-time PCR analysis. * $P<0.05$, ** $P<0.001$. Error bars indicate standard deviation.

primary neurospheres increased by 1.6-fold ($n=12$), whereas no significant differences in the number of small neurospheres were observed ($n=12$) (Fig. 5A, B). On the other hand, when the neurospheres were cultured without EGF and FGF-2, no large neurospheres were observed, even in the presence of PEDF (data not shown). It has been generally considered that large neurospheres are derived from self-renewing progenitor cells and small neurospheres are generated from progenitor cells that have more restricted self-renewal ability (Seaberg and van der Kooy, 2002). To evaluate the effect of PEDF on the self-renewal ability of progenitor cell, primary neurospheres cultured with or without PEDF (25 ng/ml) were dissociated and maintained without PEDF for 5 days to generate secondary neurospheres. The number of the large secondary neurospheres significantly increased by 1.5-fold ($n=5$) (Fig. 5C, D), suggesting that PEDF stimulates the self-renewal of progenitor cells. We next analyzed the effect of PEDF on the proliferation of progenitor cells. Using primary neurospheres, we performed a BrdU-incorporation assay and anti-phosphorylated histone H3 antibody staining. Primaly neurospheres cultured for 4 days were incubated with or without PEDF (25 ng/ml) for 12 h and were subsequently incubated with BrdU for 2 h. PEDF treatment increased the percentages of BrdU-labeled cells (Fig. 5E, F; PEDF: 42.9±3.3%, control: 21.0±1.8%, $n=4$) and phosphorylated histone H3-positive cells (Fig. 5G, H; PEDF: 11.5±2.2%, control: 4.0±0.8%, $n=4$) among the neurosphere-forming cells.

We next examined the effect of PEDF on cellular differentiation as evaluated using anti-Dcx antibody, anti-GFAP antibody and anti-O4 antibody staining. Primary neurospheres were dissociated and plated onto PLL-coated coverslips, cultured for 7 days with or without PEDF (25 ng/ml), and then allowed to differentiate by culturing for 5 days in a medium without growth factors. Since no significant differences in the percentage of neuron (Dcx+), astrocyte (GFAP+) and oligodendrocyte (O4+) after PEDF-treatment were observed (Fig. 6A, B), we confirmed that PEDF hardly affected cellular differentiation. We further investigated the effect of PEDF on multipotency of neurospheres under the clonal condition. The percentage of three types of neural lineages; Dcx/GFAP/O4, Dcx/GFAP, and GFAP, was almost similar between control and PEDF-treated neurosheres (Fig. 6C). These results suggest that PEDF enhances cellular proliferation and self-renewing but is not involved in the multilineage potency of hippocampal progenitor cells.

We next examined the effect of PEDF on cellular proliferation of hippocampal progenitor *in vivo*. AAV carrying mouse PEDF and EGFP cDNAs or carrying EGFP cDNA alone as a control was infected into the DG. The mice were injected i.p. with BrdU 7 days after the AAV-infection, and fixed 1 day after the BrdU-injection. However, there were no significant differences in the number of the BrdU-labeled cells in the granule cell layer (GCL) between PEDF-infected group and control group (Fig. 7), suggesting that PEDF *per se* does not stimulate the cellular proliferation.

DISCUSSION

Recent studies have shown that memantine promotes cellular proliferation and the production of mature granule cells in adult hippocampus (Jin et al., 2006; Maekawa et al., 2009). However, the molecular mechanism responsible for the memantine-induced promotion of cellular proliferation remains unknown. Marvanova et al. (2001) reported that memantine at a dose of 50 mg/kg, the same dose used in our study, clearly induced the expression of BDNF and its receptor TrkB in adult hippocampus, similar to our results (Fig. 3), but recent studies have revealed that BDNF signaling mainly acts on the survival of newly generated cells, rather than cellular proliferation (Sairanen et al., 2005). Additionally BDNF signaling did not affect the proliferation of hippocampal progenitor cells, unlike SVZ progenitor cells, in an *in vitro* experiment (Walker et al., 2008). Furthermore, FGF-2, a mitogen for neural stem cells in *in vitro* experiments (Reynolds and Weiss, 1992),

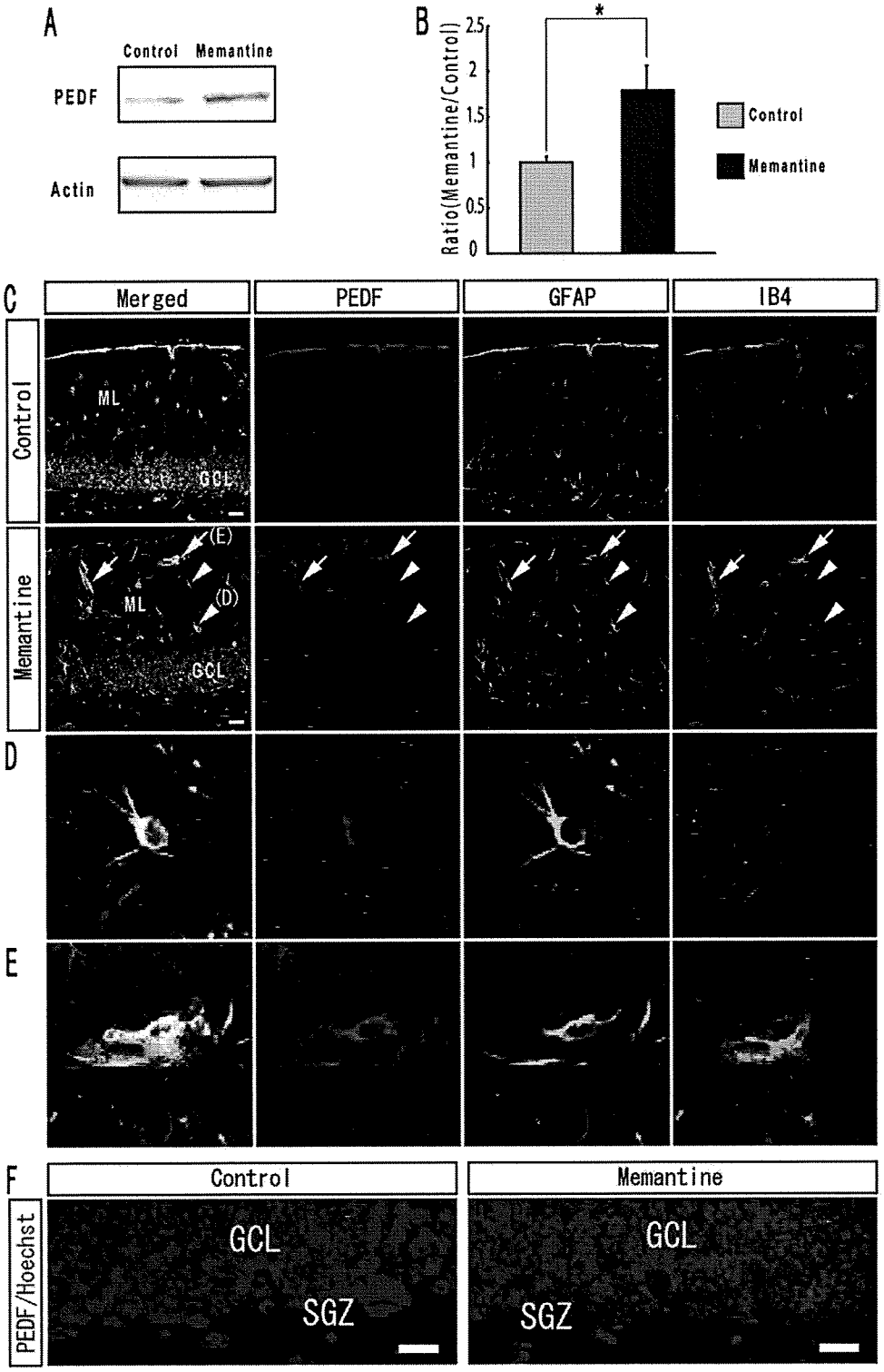

Fig. 4. Up-regulation of PEDF expression in the DG after the injection of memantine. (A) Immunoblot analysis. Three-month-old mice were injected i.p. with a dose of 50 mg/kg memantine, and cell lysate was prepared from the DG 2 days after the memantine-injection. Protein samples (30 μg) were separated using SDS-PAGE and immunoblotted with anti-PEDF antibody and ant-actin antibody as an internal control. (B) Quantitative analysis of PEDF protein expression. The ratio of PEDF protein expression (memantine-injected group/control group) was evaluated using an immunoblot analysis. * $P<0.05$. Error bars indicate standard error of the mean. (C–F) Immunohistochemical analysis. Three-month-old mice were injected i.p. with a dose of 50 mg/kg memantine, and the brains were fixed 2 days after memantine-injection. Representative examples of PEDF-positive cells (red), GFAP-positive cells (blue), and IB4-positive cells (green) in the DG at a lower magnification (C) and higher magnification (D, E). The arrows indicate endothelial cells and the arrowheads indicate astrocyte. GCL, granule cell layer; ML, molecular layer. (F) Representative examples of PEDF-positive cells (red) in the SVZ at a higher magnification. The sections were co-stained with Hoechst (blue). SGZ, subgranular zone. Scale bars=20 μm in panels C and F.

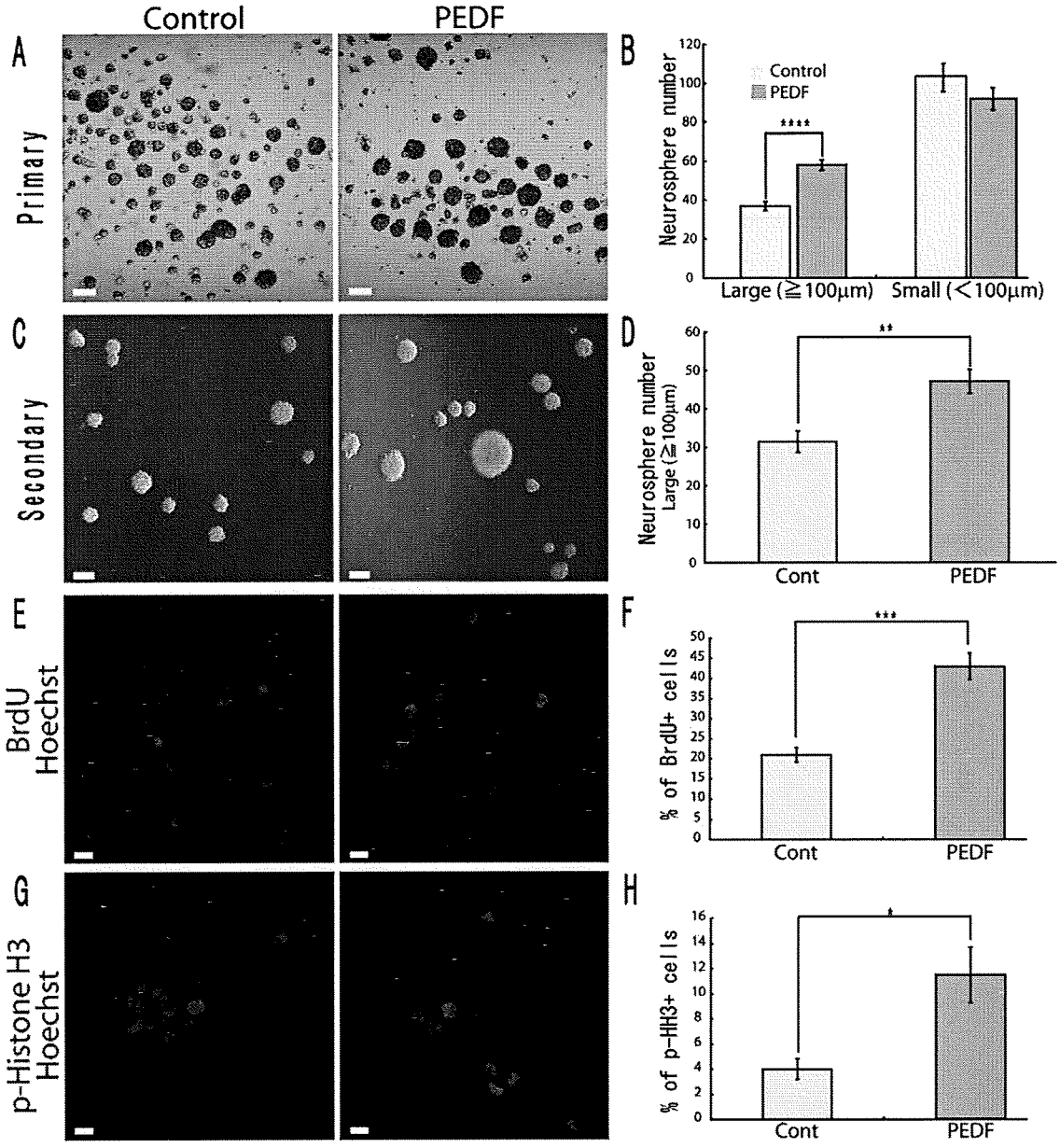

Fig. 5. Effects of PEDF on neurosphere formation, proliferation and differentiation of hippocampal progenitor cells. (A) Primary neurosphere formation. Neurospheres prepared from P1 mouse hippocampus were cultured for 7 days in the absence (control) or in the presence of PEDF (25 ng/ml). (B) Quantitative analysis of the number of primary neurospheres. (C) Secondary neurosphere formation. Primary neurospheres were generated in the absence (control) or in the presence of PEDF (25 ng/ml), passaged and then cultured for 5 days to generate secondary neurospheres. (D) Quantitative analysis of the number of secondary neurospheres. (E, G) Immunocytochemical experiments. Neurospheres cultured for 4 days were maintained in the absence (control) or in the presence of PEDF (25 ng/ml) for 12 h, and subsequently incubated with BrdU for 2 h. After washing, they were immunostained with anti-BrdU antibody (red in E) or anti-phosphorylated histone H3 (p-Histone H3) antibody (red in G). The cells were co-stained with Hoechst (blue). (F, H) Quantitative analysis of the percentage of BrdU-labeled cells (F) and p-Histone H3-positive cells (H). * $P<0.05$, ** $P<0.01$, *** $P<0.001$ and **** $P<0.00001$, when compared with the control culture. Scale bars=100 μm in panels A and C, 10 μm in panels E and G. Error bars indicate standard error of the mean.

was also up-regulated by the injection of memantine in adult hippocampus (Fig. 3 and Namba et al., 2009). *In vivo* experiments, however, have showed that FGF-2 failed to stimulate the proliferation of hippocampal progenitor cells in the young adult mice (Kuhn et al., 1997; Wagner et al., 1999; Jin et al., 2003). Therefore, distinct factors likely mediate the effect of memantine on cellular proliferation in adult hippocampus. In the present study, we found that the expression of PEDF was dramatically increased by the injection of memantine in adult hippocampus. PEDF was initially identified as a differentiating factor for retinoblastoma cells (Tombran-Tink et al., 1991), and later studies have shown that it also has neurotrophic and neuroprotective functions in various neuronal populations, as well as

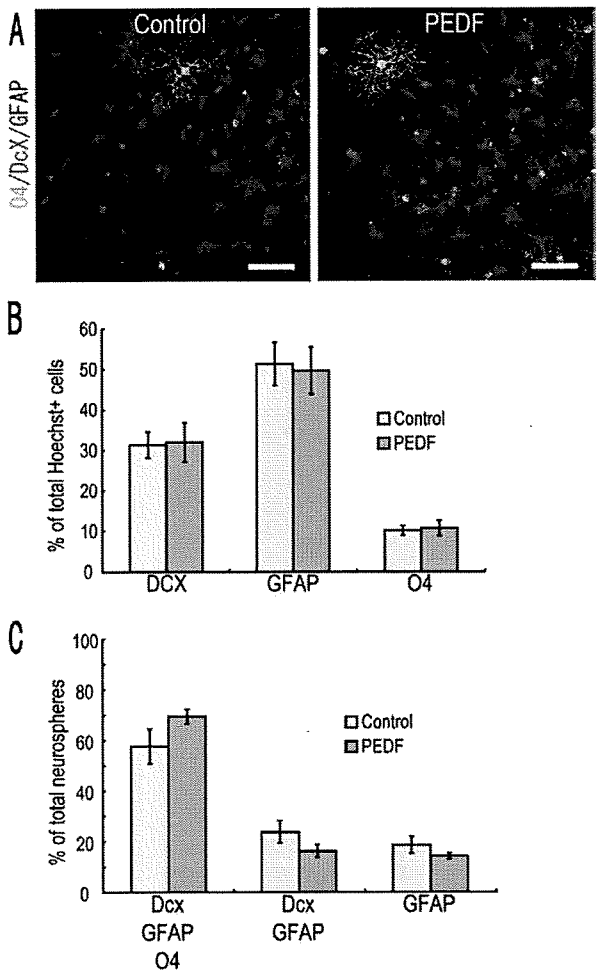

Fig. 6. Differentiation of hippocampal progenitor cells. (A) Representative immunohistochemical staining with anti-O4 antibody (green), anti-Dcx antibody (red) and anti-GFAP antibody (blue). Scale bars=50 μm. (B) Quantitative analysis of the percentage of Dcx-positive cells, GFAP-positive cells and O4-positive cells. (C) Quantitative analysis of the percentage of three types of neural lineages; Dcx/GFAP/O4, Dcx/GFAP, and GFAP. Error bars indicate standard error of the mean.

acting as a potent anti-angiogenic factor (Tombran-Tink and Barnstable, 2003; Sanagi et al., 2008). Interestingly, recent studies have shown that the expression of PEDF is increased by ischemic insult and antidepressant treatment (Miller et al., 2008; Sanagi et al., 2008). Neurogenesis is known to be enhanced under these conditions (Malberg et al., 2000; Tanaka et al., 2004). Furthermore, Ramirez-Castillejo et al. (2006) reported that PEDF increased the number of neurospheres derived from adult SVZ but did not affect the average size of the neurospheres. In the present study using hippocampal neurospheres, we also showed that PEDF increased the number of large neurospheres and enhanced the proliferation of progenitor cells in the presence of EGF and FGF-2 but did not stimulate their proliferation in the absence of EGF and FGF-2. In accordance with the results of *in vitro* study, PEDF expressed by using AAV did not stimulate the cellular proliferation *in vivo*. These results suggest that PEDF is an enhancing molecule for the proliferation of hippocampal progenitor cells in the presence of mitogens such as FGF-2 and EGF. Moreover, PEDF did not affect the average size of the large neurospheres (data not shown). These findings are similar to previous results obtained in the SVZ (Ramirez-Castillejo et al., 2006), suggesting that PEDF is a potent microenvironmental factor for neural progenitor cells in the two major neurogenic regions: the hippocampus and the SVZ.

Ramirez-Castillejo et al. (2006) reported that PEDF was released from lectin IB4-positive endothelial cells and S100β-positive ependymal cells in the SVZ but not expressed by SVZ progenitor cells. Furthermore, PEDF increased the expression of Notch effectors Hes1 and Hes5 in neuronal progenitor cells (Ramirez-Castillejo et al., 2006). Our previous study using the neocortices of mouse embryos also showed that an NMDA receptor antagonist promoted the proliferation of progenitor cells in the SVZ and increased the expression of Hes1 and Hes5 (Hirasawa et al., 2003). In the hippocampus, however, an immunohistochemical study demonstrated that PEDF was expressed in the GFAP-positive protoplasmic and perivascular astrocytes (Fig. 4) and hippocampal progenitor cells *in vitro* (data not shown), and neither increases in the expression of Hes1 nor Hes5 were detected after the injection of memantine (data not shown). Thus, the mechanism by which PEDF increases the proliferation of progenitor cells might differ between the hippocampus and the SVZ.

Memantine has been used clinically as a neuroprotective agent to treat moderate-to-severe Alzheimer's disease (AD). In clinical practice, a stable dose of memantine (20 mg/day) has been found to produce a steady-state plasma memantine level of approximately 0.5 μM in AD patients (Kornhuber and Quack, 1995). In rodent, the oral administration of memantine (30 mg/kg daily for 5 weeks) produced a steady-state plasma memantine concentration of ~1 μM, and it improved spatial learning in a transgenic mouse model of AD (Minkeviciene et al., 2004). In addition, the administration of memantine by an intragastric route (7.5 mg/kg daily for 2 weeks) increased the proliferation of progenitor cells in the hippocampus (Jin et al., 2006). Interestingly, a higher oral dose of memantine (100 mg/kg daily for 4 weeks), which produced a steady-state plasma memantine concentration of approximately 6 μM (>10-fold higher than clinical level), improved cognition and had a potential anxiolytic response in mice (Minkeviciene et al., 2008), suggesting that the different ranges of memantine dose result in different pharmacological effects although adverse effects in rodent have not been elucidated. By contrast, in case of an acute administration of memantine such as by i.p. injection, since a 2.5–5.0 mg/kg dose of memantine produced a plasma memantine concentration of approximately 1 μM (Danysz et al., 1997), the 50 mg/kg i.p. dose of memantine used in our experiments likely produced a higher plasma memantine concentration (probably >10-fold higher than the concentration of a therapeutic dose), and we found that only higher dose of memantine increased both the proliferation of progenitor cells and the expression level of PEDF. To elucidate the molecular mechanism responsible for memantine-in-

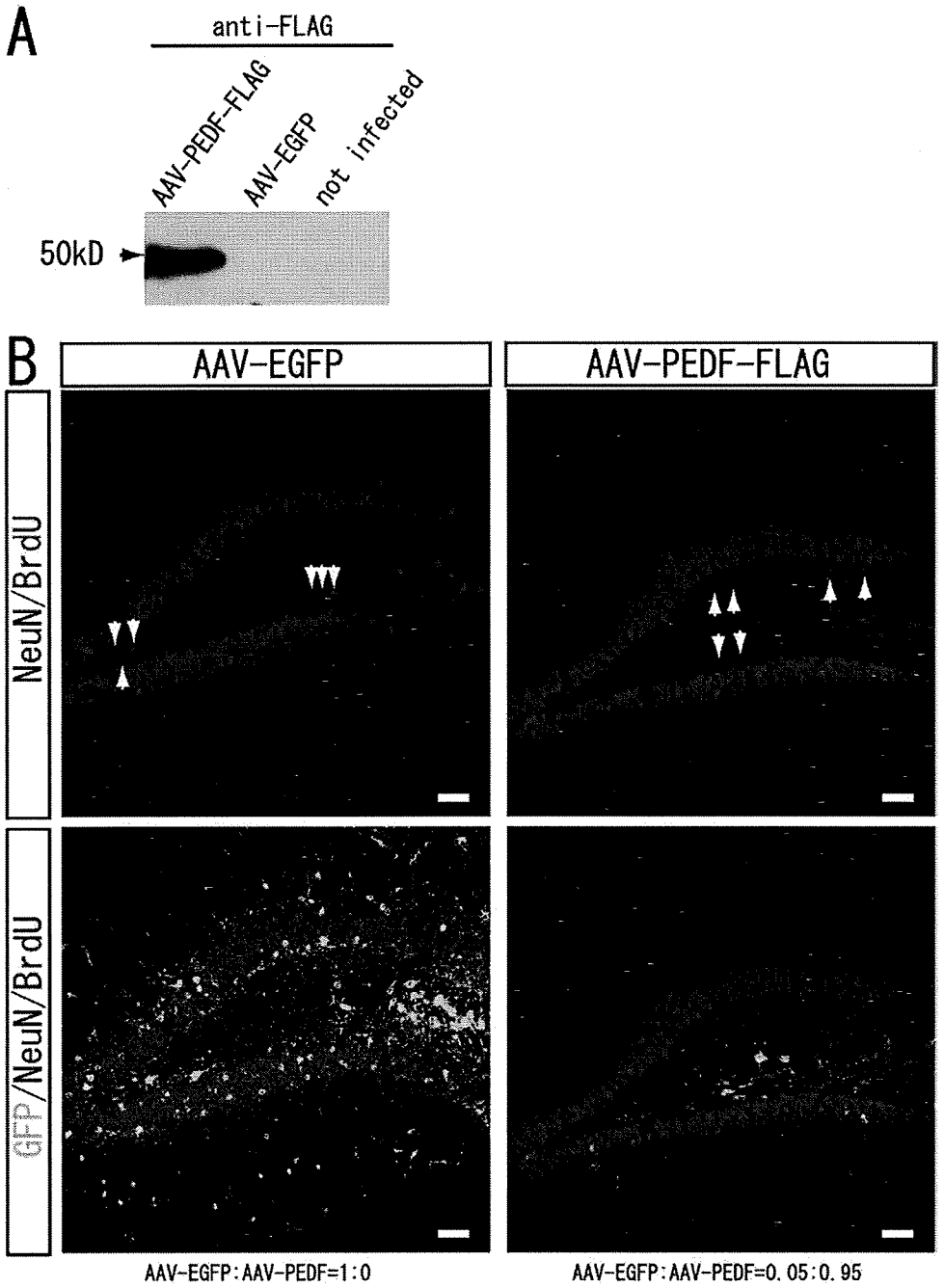

Fig. 7. Effect of PEDF on cellular proliferation in the DG. (A) Immunoblotting with anti-FLAG antibody. AAV-mPEDF or AAV-GFP was infected into COS7 cells, and equal amounts of culture media were subjected to immunoblot analysis. (B) Representative examples of BrdU-labeled cells (red) shown by arrowheads. Three-month-old mice were infected with AAV-mPEDF and AAV-EGFP or AAV-EGFP alone, and then injected i.p. with BrdU 7 days after the AAV-infection. The mice were fixed one day after the BrdU-injection. The sections were co-stained with anti-NeuN antibody (blue). AAV-infected cells were visualized by EGFP signals. Scale bars=50 μm.

duced PEDF up-regulation, we will need further studies including the investigation of PEDF expression under the same condition as clinical practice.

CONCLUSION

In conclusion, to clarify the molecular bases of the promotion of cell proliferation by memantine, we searched for a factor that mediates memantine-induced cellular proliferation, and found that PEDF is up-regulated in the DG of adult mice after the memantine-injection. Using neurosphere assay we confirmed that PEDF enhanced the cellular proliferation but was not involved in the multilineage potency of hippocampal progenitor cells. Since present and previous studies have shown that neither PEDF nor

FGF-2 *per se* stimulated cellular proliferation *in vivo*, it can be speculated that simultaneous up-regulation of PEDF and FGF-2 after the memantine treatment leads the synergistic effects on progenitor cell proliferation *in vivo*.

Acknowledgments—We very thank Dr. Kozo Kaibuchi for useful discussion, Dr. Yusuke Tozuka for useful advice, Dr. Toru Yasuda and Ms. Tomoko Nihira for AAV preparation and Dr. Ikuo Morita for generous gift of mouse PEDF cDNA. This work was supported by The Ministry of Health, Labour and Welfare of Japan, The Program for the Promotion of Fundamental Studies in Health Science of the National Institute of Biomedical Innovation.

REFERENCES

Altman J, Das GD (1965) Autoradiographic and histological evidence of postnatal hippocampal neurogenesis in rats. J Comp Neurol 124:319–335.

Alvarez-Buylla A, Seri B, Doetsch F (2002) Identification of neural stem cells in the adult vertebrate brain. Brain Res Bull 57:751–758.

Danysz W, Parsons CG, Kornhuber J, Schmidt WJ, Quack G (1997) Aminoadamantanes as NMDA receptor antagonists and antiparkinsonian agents—preclinical studies. Neurosci Biobehav Rev 21:455–468.

Eriksson PS, Perfilieva E, Bjork-Eriksson T, Alborn AM, Nordborg C, Peterson DA, Gage FH (1998) Neurogenesis in the adult human hippocampus. Nat Med 4:1313–1317.

Hattori K, Uchino S, Isosaka T, Maekawa M, Iyo M, Sato T, Kohsaka S, Yagi T, Yuasa S (2006) Fyn is required for haloperidol-induced catalepsy in mice. J Biol Chem 281:7129–7135.

Hirasawa T, Wada H, Kohsaka S, Uchino S (2003) Inhibition of NMDA receptors induces delayed neuronal maturation and sustained proliferation of progenitor cells during neocortical development. J Neurosci Res 74:676–687.

Hosomichi J, Yasui N, Koide T, Soma K, Morita I (2005) Involvement of the collagen I-binding motif in the anti-angiogenic activity of pigment epithelium-derived factor. Biochem Biophys Res Commun 335:756–761.

Jin K, Sun Y, Xie L, Batteur S, Mao XO, Smelick C, Logvinova A, Greenberg DA (2003) Neurogenesis and aging: FGF-2 and HB-EGF restore neurogenesis in hippocampus and subventricular zone of aged mice. Aging Cell 2:175–183.

Jin K, Xie L, Mao XO, Greenberg DA (2006) Alzheimer's disease drugs promote neurogenesis. Brain Res 1085:183–188.

Kodomari I, Wada E, Nakamura S, Wada K (2009) Maternal supply of BDNF to mouse fetal brain through the placenta. Neurochem Int 54:95–98.

Kornhuber J, Quack G (1995) Cerebrospinal fluid and serum concentrations of the N-methyl-D-aspartate (NMDA) receptor antagonist memantine in man. Neurosci Lett 195:137–139.

Kuhn HG, Winkler J, Kempermann G, Thal LJ, Gage FH (1997) Epidermal growth factor and fibroblast growth factor-2 have different effects on neural progenitors in the adult rat brain. J Neurosci 17:5820–5829.

Maekawa M, Namba T, Suzuki E, Yuasa S, Kohsaka S, Uchino S (2009) NMDA receptor antagonist memantine promotes cell proliferation and production of mature granule neurons in the adult hippocampus. Neurosci Res 63:259–266.

Maekawa M, Takashima N, Arai Y, Nomura T, Inokuchi K, Yuasa S, Osumi N (2005) Pax6 is required for production and maintenance of progenitor cells in postnatal hippocampal neurogenesis. Genes Cells 10:1001–1014.

Malberg JE, Eisch AJ, Nestler EJ, Duman RS (2000) Chronic antidepressant treatment increases neurogenesis in adult rat hippocampus. J Neurosci 20:9104–9110.

Marvanova M, Lakso M, Pirhonen J, Nawa H, Wong G, Castren E (2001) The neuroprotective agent memantine induces brain-derived neurotrophic factor and trkB receptor expression in rat brain. Mol Cell Neurosci 18:247–258.

Miller BH, Schultz LE, Gulati A, Cameron MD, Pletcher MT (2008) Genetic regulation of behavioral and neuronal responses to fluoxetine. Neuropsychopharmacology 33:1312–1322.

Ming GL, Song H (2005) Adult neurogenesis in the mammalian central nervous system. Annu Rev Neurosci 28:223–250.

Minkeviciene R, Banerjee P, Tanila H (2004) Memantine improves spatial learning in a transgenic mouse model of Alzheimer's disease. J Pharmacol Exp Ther 311:677–682.

Minkeviciene R, Banerjee P, Tanila H (2008) Cognition-enhancing and anxiolytic effects of memantine. Neuropharmacology 54:1079–1085.

Namba T, Maekawa M, Yuasa S, Kohsaka S, Uchino S (2009) The Alzheimer's disease drug memantine increases the number of radial glia-like progenitor cells in adult hippocampus. Glia 57:1082–1090.

Namba T, Mochizuki H, Onodera M, Mizuno Y, Namiki H, Seki T (2005) The fate of neural progenitor cells expressing astrocytic and radial glial markers in the postnatal rat dentate gyrus. Eur J Neurosci 22:1928–1941.

Petrus DS, Fabel K, Kronenberg G, Winter C, Steiner B, Kempermann G (2009) NMDA and benzodiazepine receptors have synergistic and antagonistic effects on precursor cells in adult hippocampal neurogenesis. Eur J Neurosci 29:244–252.

Ramirez-Castillejo C, Sanchez-Sanchez F, Andreu-Agullo C, Ferron SR, Aroca-Aguilar JD, Sanchez P, Mira H, Escribano J, Farinas I (2006) Pigment epithelium-derived factor is a niche signal for neural stem cell renewal. Nat Neurosci 9:331–339.

Reynolds BA, Weiss S (1992) Generation of neurons and astrocytes from isolated cells of the adult mammalian central nervous system. Science 255:1707–1710.

Sairanen M, Lucas G, Ernfors P, Castren M, Castren E (2005) Brain-derived neurotrophic factor and antidepressant drugs have different but coordinated effects on neuronal turnover, proliferation, and survival in the adult dentate gyrus. J Neurosci 25:1089–1094.

Sanagi T, Yabe T, Yamada H (2007) Changes in pigment epithelium-derived factor expression following kainic acid induced cerebellar lesion in rat. Neurosci Lett 424:66–71.

Sanagi T, Yabe T, Yamada H (2008) Gene transfer of PEDF attenuates ischemic brain damage in the rat middle cerebral artery occlusion model. J Neurochem 106:1841–1854.

Seaberg RM, van der Kooy D (2002) Adult rodent neurogenic regions: the ventricular subependyma contains neural stem cells, but the dentate gyrus contains restricted progenitors. J Neurosci 22:1784–1793.

Seki T, Arai Y (1993) Highly polysialylated neural cell adhesion molecule (NCAM-H) is expressed by newly generated granule cells in the dentate gyrus of the adult rat. J Neurosci 13:2351–2358.

Seki T, Namba T, Mochizuki H, Onodera M (2007) Clustering, migration, and neurite formation of neural precursor cells in the adult rat hippocampus. J Comp Neurol 502:275–290.

Tanaka R, Yamashiro K, Mochizuki H, Cho N, Onodera M, Mizuno Y, Urabe T (2004) Neurogenesis after transient global ischemia in the adult hippocampus visualized by improved retroviral vector. Stroke 35:1454–1459.

Tombran-Tink J, Barnstable CJ (2003) PEDF: a multifaceted neurotrophic factor. Nat Rev Neurosci 4:628–636.

Tombran-Tink J, Chader GG, Johnson LV (1991) PEDF: a pigment epithelium-derived factor with potent neuronal differentiative activity. Exp Eye Res 53:411–414.

Tozuka Y, Fukuda S, Namba T, Seki T, Hisatsune T (2005) GABAergic excitation promotes neuronal differentiation in adult hippocampal progenitor cells. Neuron 47:803–815.

Wagner JP, Black IB, DiCicco-Bloom E (1999) Stimulation of neonatal and adult brain neurogenesis by subcutaneous injection of basic fibroblast growth factor. J Neurosci 19:6006–6016.

Walker TL, White A, Black DM, Wallace RH, Sah P, Bartlett PF (2008) Latent stem and progenitor cells in the hippocampus are activated by neural excitation. J Neurosci 28:5240–5247.

Yabe T, Kanemitsu K, Sanagi T, Schwartz JP, Yamada H (2005) Pigment epithelium-derived factor induces pro-survival genes through cyclic AMP-responsive element binding protein and nuclear factor kappa B activation in rat cultured cerebellar granule cells: implication for its neuroprotective effect. Neuroscience 133:691–700.

Yasuda T, Miyachi S, Kitagawa R, Wada K, Nihira T, Ren YR, Hirai Y, Ageyama N, Terao K, Shimada T, Takada M, Mizuno Y, Mochizuki H (2007) Neuronal specificity of alpha-synuclein toxicity and effect of Parkin co-expression in primates. Neuroscience 144:743–753.

(Accepted 19 January 2010)
(Available online 28 January 2010)

Glycobiology vol. 19 no. 9 pp. 1018–1033, 2009
doi:10.1093/glycob/cwp083
Advance Access publication on June 18, 2009

Unusual accumulation of sulfated glycosphingolipids in colon cancer cells

Kyoko Shida[2], Yoshiko Misonou[2], Hiroaki Korekane[3], Yosuke Seki[4], Shingo Noura[4], Masayuki Ohue[4], Koichi Honke[5,6,7], and Yasuhide Miyamoto[1,2]

[2]Department of Immunology, Osaka Medical Center for Cancer and Cardiovascular Diseases, 1-3-2 Nakamichi, Higashinari-ku, Osaka 537-8511; [3]Department of Disease Glycomics, The Institute of Scientific and Industrial Research, Osaka University, 8-1 Mihogaoka, Ibaraki, Osaka 567-0047; [4]Department of Surgery, Osaka Medical Center for Cancer and Cardiovascular Diseases, 1-3-3 Nakamichi, Higashinari-ku, Osaka 537-8511; [5]Department of Biochemistry; [6]Kochi System Glycobiology Center, Kochi University Medical School, Nankoku, Kochi 783-8505; and [7]CREST, Japan Science and Technology Agency, Kawaguchi, Japan

Received on April 30, 2009; revised on June 5, 2009; accepted on June 8, 2009

The structures of glycosphingolipids from highly purified colorectal cancer cells and normal colorectal epithelial cells of 16 patients have been analyzed in fine detail (Misonou Y, Shida K, Korekane H, Seki Y, Noura S, Ohue M, Miyamoto Y. 2009. Comprehensive Clinico-Glycomic Study of 16 Colorectal Cancer Specimens: Elucidation of aberrant glycosylation and ts mechanistic causes in colorectal cancer cells. *J Proteome Res.* 8:2990–3005). Further structural analyses demonstrated that colon cancer cells from two patients accumulated unusual glycosphingolipids which were not observed in either colorectal cancer cells or normal colorectal epithelial cells from the other patients. Mass spectrometry analyses revealed that the unusual structures include sulfated oligosaccharides. The structures of the glycosphingolipids of the cancer cells from these two cases were analyzed by methods which include enzymatic release of carbohydrate moieties, fluorescent labeling with aminopyridine and identification using two-dimensional mapping, enzymatic digestion and mass spectrometry together with methanolysis, and the use of newly synthesized sulfo-fucosylated oligosaccharides as standards. The colon cancer cells from one of the patients demonstrate a variety of oligosaccharides as major components which are sulfated at the C6 position of subterminal GlcNAc and at C3 positions of terminal galactose with or without sialylation or fucosylation. These include 6-sulfo Le^x, 6′-sialyl 6-sulfo lactosamine, and 3′-sialyl 6-sulfo Le^x, in addition to sialylated or fucosylated derivatives of type-1 and type-2 hybrid oligosaccharides. The colon cancer cells from the other patient have two kinds of sulfated oligosaccharides, a 6-sulfo Le^x structure and a 3′-sulfo Le^x structure, as minor components. Taking into consideration the clinical features of the two patients, the biological significance of sulfated glycosphingolipids on cancer cells is discussed.

[1]To whom correspondence should be addressed: Tel: +81-6-6972-1181; Fax: +81-6-6972-7749; e-mail: miyamoto-ya@mc.pref.osaka.jp

Keywords: colon cancer/glycosphingolipid/sulfate/two-dimensional mapping

Introduction

Malignant transformation is frequently accompanied by a drastic alteration in the structures of oligosaccharides of the cell surface (Hakomori 1989, 2002). Subsequent series of studies have indicated the functional significance of aberrant glycosylation in cancer malignancy, such as metastasis and invasion (Hakomori 1996, 2002; Ono and Hakomori 2004). In our recent study, in order to pursue the association between aberrant glycosylation and cancer malignancy, we comprehensively and precisely analyzed the structures of glycosphingolipids (GSLs) from highly purified colorectal cancer cells (CCs) and normal colorectal epithelial cells (NCs) of 16 patients (Misonou et al. 2009). We reported the alteration in the structures of GSLs in carcinogenesis in general and that characteristic patterns tend to be associated with clinical features such as hepatic metastasis (Misonou et al. 2009). In brief, GSLs of human NCs are mostly composed of neutral GSLs, such as LacCer and Le^a. Three specific alterations were observed in malignant transformation, namely increased ratios of type-2 oligosaccharides, increased α2-3 and/or α2-6 sialylation, and increased α1-2 fucosylation. These alterations result in increases in the amount of or appearance of Le^x, LST-c, Le^y, Le^b, sialyl Le^x, sialyl Le^a, IV^{6}NeuAcαIV^{2}Fucα-nLc$_4$, V^{3}FucαIII^{3}Fucα-nLc$_6$, VI^{3}NeuAcα-nLc$_6$, and VI^{6}NeuAcαIII^{3}Fucα-nLc$_6$. Furthermore, a shift from type-1 dominant NCs to type-2 dominant CCs was found in the five cases having hepatic metastasis. We have subsequently analyzed the structures of GSLs from CCs and NCs to increase the number of analyzed cases in order to confirm the findings previously reported and to further investigate other characteristic alterations associated with other clinical features such as lung metastasis, invasion to adjacent tissues, and low metastatic potential. While similar results to those previously reported were obtained in most cases, we found that the CCs from two cases accumulated unusual GSLs, which were not found in CCs and NCs of the other cases. Taking into consideration the clinical features, such as tumor size, depth of invasion, metastasis to lymph node, and long distance organs, both cases are estimated to have low metastatic potential. Tandem mass spectrometry analyses of these unusual oligosaccharides revealed that CCs from both patients include sulfated GSLs, most of which were sialylated and/or fucosylated, and one set of CCs include isomers of GSLs normally observed in CCs.

Human tissues contain varieties of sulfoglycolipids, such as SM4s, SM4g, SM3, SMGb4, SMGb5, SMUnLc$_4$, and SMUnLc$_6$, and the presence of SM3 and SM4 in colon cancer tissues has been reported from our and other laboratories (Fukushi et al. 1984; Ishizuka 1997; Korekane et al. 2007).

Table I. Clinicopathological information on the two patients with colon adenocarcinoma

No	Age	Sex	Tumor localization	Tumor size (mm)	Histological differentiation	Depth of invasion	LN[a]	LM[a]	Blood type	CEA (ng/mL)	CA19–9 (U/mL)
1	64	M	Sigmoid	100 × 120	Moderately	Si[a] (urinary bladder)	N0	H0	A	9.8	27
2	76	M	Ascending	88 × 40	Moderately	SS[a]	N0	H0	A	3.7	16

[a]LN, lymph node metastasis; LM, liver metastasis; SS, subserosa; Si, invasion to neighboring tissue.

However, the structures of the unusual sulfoglycolipids found in the CCs in these two cases have not been reported to date.

Carbohydrate sulfation occurs in a number of biological compounds, such as proteoglycans, glycoproteins, and GSLs, and the biological significance of sulfation of carbohydrates has been demonstrated in a variety of systems including the reproductive system, immune system, and embryonic development (Bullock et al. 1998; Forsberg et al. 1999; Humphries et al. 1999; Tangemann et al. 1999; Hemmerich et al. 2001; Honke et al. 2002). However, the involvement of the accumulation of sulfated carbohydrates in cancer malignancy has not been well studied.

In this study, we elucidate the fine structures of the major GSLs of CCs and NCs from the two patients which include a variety of sulfated GSLs. The significance of the sulfated GSLs is considered in *Discussion*.

Results

Preparation of PA-oligosaccharides from CD326-positive colon adenocarcinoma cells and normal colon epithelial cells from two colon cancer patients

The clinicopathological features of the two patients are described in Table I. The colon cancer in case 1 is thought to have very low metastatic potential because it was very large (100 × 120 mm), invaded the bladder but did not metastasize to lymph nodes and long-distance organs such as liver and lung (Table I). More than 2 years have passed since removal of the primary colon cancer and bladder by operation, but there has been no recurrence in this case. The colon cancer in case 2 is also thought to have low metastatic potential. The size of the primary cancer was 80 mm × 41 mm and invaded the subserosa, but no lymph node or long-distance metastasis were detected, as in case 1 (Table I). No recurrence was found in this case either. PA-oligosaccharides of GSLs were prepared from CCs and NCs from the two cases (cases 1 and 2), which were isolated with high purity from the colon cancer tissues and surrounding normal colon epithelial tissues using magnetic beads labeled with antibody against the epithelial cell marker, CD326.

Structural analysis of PA-oligosaccharides of case 1

The neutral and acidic PA-oligosaccharides from purified CCs and NCs from case 1 were analyzed by size-fractionation high-performance liquid chromatography (HPLC) (Figure 1). Fifteen (N1–N15) and 23 peaks (A1–A23) were obtained from neutral and acidic GSLs of the CCs, respectively (Figure 1**C** and **A**), and two peaks (N1 and N7–1) and three peaks (A1, A2, and A9) from neutral and acidic GSLs of NCs (Figure 1**D** and **B**). The profiles of both acidic and neutral GSLs from NCs from this patient are similar to those from the colon cancer patients as reported in our recent paper (Figure 1**B** and **D**). Thus, the neutral GSLs are mainly composed of lactose and Le^a (N1 and N7–1 in Figure 1**D**) and acidic GSLs composed of SM3, GM3 with LSTc as a very minor component (A1, A2, and A9 in Figure 1**B**). In contrast, the profile of GSLs, especially the acidic fraction, from CCs from this patient shows a variety of peaks in addition to the common characteristic peaks of CCs. Peaks in the neutral and acidic GSLs, A1, A2, A4, A9, A11, A12, A16, A22, A23, N1, N2, N3, N5, N7, N9, N10, N11, N15 (closed arrows), are observed in CCs from many cases. However, the other peaks (open arrow) have rarely been observed in human CCs. The structures of all the major peaks observed from the CCs were analyzed by a combination of a 2D mapping technique, enzymatic digestion, methanolysis, and mass spectrometry analyses as described below.

Each of the peaks was further purified by reversed-phase HPLC. Peaks N7, N10, N12, N13, A10, A13, and A16 were separated into two major components in reversed-phase HPLC, and each designated N7-1, N7-2, N10-1, N10-2, N12-1, N12-2, N13-1, N13-2, A10-1, A10-2, A13-1, A13-2, A16-1, and A16-2. Additionally, purified PA-oligosaccharides were subjected to LC/ESI MS/MS. Elution positions of N1–N15 and A1–A23 on size fractionation and reversed-phase HPLC are summarized in Figure 2 as a 2D map.

From comparison of the positions on the map to the positions of standard PA-oligosaccharides, N1, N2, N3, N4, N5, N6, N7-1, N7-2, N8, N9, N10-1, N11, N12-1, N14, N15, A1, A2, A3, A4, A7, A8, A9, A11, A12, A16-1, A22, and A23 are predicted to be lactose, Lc_3, Globo-*N*-tetraose (Gb_4), lacto-*N*-tetraose (Lc_4), lacto-*N*-neotetraose (nLc_4), lacto-*N*-fucopentaose I (Type I H), lacto-*N*-fucopentaose II (Le^a), lacto-*N*-fucopentaose III (Le^x), A-hexasaccharide (Type I A), Le^y-hexasaccaharide (Le^y), Le^b-hexasaccaharide (Le^b), lacto-*N*-neohexasaccharide (nLc_6), A-heptasaccharide (ALe^b), $III^3Fuc\alpha$-nLc_6, $V^3Fuc\alpha III^3Fuc\alpha$-$nLc_6$, SM3, GM3, 3′-sulfo-$Lc_4$, GD3, LST-a, LST-b, LST-c, SLe^x, SLe^a, $VI^3NeuAc\alpha$-nLc_6, $VI^6NeuAc\alpha III^3Fuc\alpha$-nLc6, and $VI^3NeuAc\alpha V^3Fuc\alpha III^3Fuc\alpha$-nLc6, respectively (Figure 2). The structures of these 2D matched oligosaccharides were also confirmed by mass spectrometry. Fractions N10-2, N12-2, N13-1, N13-2, A5, A6, A10-1, A10-2, A13-1, A13-2, A14, A15, A16-2, A17, A18, A19, A20, and A21 do not match any of the reference compounds on the 2D map accumulated prior to our studies. Elution positions, mass data, and estimated composition of these unmatched oligosaccharides are presented in Table III. In the following results sections, the structures of these PA-oligosaccharides are explained in detail.

Structure of N10-2, N12-2, and N13-2

MS^2 analysis revealed that N10-2 has a lacto or neolacto series hexasaccharide structure, Hex-HexNAc-Hex-HexNAc-Hex-Hex-PA, but the position of N10-2 on the 2D map does not match to nLc_6. N10-2 was digested with lacto-*N*-biosidase, and the products of the digestion ran as two peaks by HPLC, corresponding to Galβ1-4Glc-PA and

Table II. Structures and elution positions in HPLC of standard PA-oligosaccharides

Abbreviation	Structure	Elution position in HPLC	
		Size (Gu)	RP (Gu)
Lactose	Galβ1-4Glc-PA	2.03	0.93
Lc_3	GlcNAcβ1-3Galβ1-4Glc-PA	2.76	2.11
Gb_4	GalNAcβ1-3Galα1-4Galβ1-4Glc-PA	3.47	2.71
Lc_4	Galβ1-3GlcNAcβ1-3Galβ1-4Glc-PA	3.66	2.50
nLc_4	Galβ1-4GlcNAcβ1-3Galβ1-4Glc-PA	3.74	2.16
TypeI H	Fucα1-2Galβ1-3GlcNAcβ1-3Galβ1-4Glc-PA	4.23	2.86
Le^a	Galβ1-3GlcNAcβ1-3Galβ1-4Glc-PA 4 | Fucα1	4.51	2.01
Le^x	Galβ1-4GlcNAcβ1-3Galβ1-4Glc-PA 3 | Fucα1	4.51	1.99
TypeI A	GalNAcα1-3Galβ1-3GlcNAcβ1-3Galβ1-4Glc-PA 2 | Fucα1	4.67	3.89
Le^y	Fucα1-2Galβ1-4GlcNAcβ1-3Galβ1-4Glc-PA 3 | Fucα1	4.98	2.96
Le^b	Fucα1-2Galβ1-3GlcNAcβ1-3Galβ1-4Glc-PA 4 | Fucα1	5.21	1.42
nLc_6	Galβ1-4GlcNAcβ1-3Galβ1-4GlcNAcβ1-3Galβ1-4Glc-PA	5.38	2.93
ALe^b	GalNAcα1-3Galβ1-3GlcNAcβ1-3Galβ1-4Glc-PA 2 4 | | Fucα1 Fucα1	5.73	1.91
$III^3Fuc\alpha\text{-}nLc_6$	Galβ1-4GlcNAcβ1-3Galβ1-4GlcNAcβ1-3Galβ1-4Glc-PA 3 | Fucα1	6.23	2.51
$V^3Fuc\alpha,III^3Fuc\alpha\text{-}nLc_6$	Galβ1-4GlcNAcβ1-3Galβ1-4GlcNAcβ1-3Galβ1-4Glc-PA 3 3 | | Fucα1 Fucα1	6.99	2.14
SM3	HSO_3-3Galβ1-4Glc-PA	1.19	2.60
GM3	Neu5Acα2-3Galβ1-4Glc-PA	2.46	3.00
3′-Sulfo-Lc_4	HSO_3-3Galβ1-3GlcNAcβ1-3Galβ1-4Glc-PA	2.74	4.25
GD3	Neu5Acα2-8Neu5Acα2-3Galβ1-4Glc-PA	3.31	4.50
GM1	Galβ1-3GalNAcβ1-4Galβ1-4Glc-PA 3 | Neu5Acα2	3.85	2.92
LST-a	Neu5Acα2-3Galβ1-3GlcNAcβ1-3Galβ1-4Glc-PA	4.01	4.69
LST-b	Galβ1-3GlcNAcβ1-3Galβ1-4Glc-PA 6 | Neu5Acα2	4.18	3.10
LST-c	Neu5Acα2-6Galβ1-4GlcNAcβ1-3Galβ1-4Glc-PA	4.40	3.76

Table II. Continued

Abbreviation	Structure	Elution position in HPLC Size (Gu)	RP (Gu)
GD1b	Galβ1-3GalNAcβ1-4Galβ1-4Glc-PA 3 Neu5Acα2-8Neu5Acα2	4.64	3.96
SLe^x	Neu5Acα2-3Galβ1-4GlcNAcβ1-3Galβ1-4Glc-PA 3 Fucα1	4.75	4.08
SLe^a	Neu5Acα2-3Galβ1-3GlcNAcβ1-3Galβ1-4Glc-PA 4 Fucα1	4.92	4.77
$VI^3NeuAc\alpha\text{-}nLc_6$	Neu5Acα2-3Galβ1-4GlcNAcβ1-3Galβ1-4GlcNAcβ1-3Galβ1-4Glc-PA	5.51	5.64
$VI^6NeuAc\alpha,III^3Fuc\alpha\text{-}nLc_6$	Neu5Acα2-6Galβ1-4GlcNAcβ1-3Galβ1-4GlcNAcβ1-3Galβ1-4Glc-PA 3 Fucα1	6.71	4.19
$VI^3NeuAc\alpha,V^3Fuc\alpha,III^3Fuc\alpha\text{-}nLc_6$	Neu5Acα2-3Galβ1-4GlcNAcβ1-3Galβ1-4GlcNAcβ1-3Galβ1-4Glc-PA 3 3 Fucα1 Fucα1	7.04	4.16
$3'\text{-Sulfo-}V^3Fuc\alpha,III^3Fuc\alpha\text{-}nLc_6$	HSO_3-3Galβ1-4GlcNAcβ1-3Galβ1-4GlcNAcβ1-3Galβ1-4Glc-PA 3 3 Fucα1 Fucα1	5.80	3.37
$3'\text{-Sulfo-}V^3Fuc\alpha,III^4Fuc\alpha\text{-}_{1,2}Lc_6$	HSO_3-3Galβ1-4GlcNAcβ1-3Galβ1-3GlcNAcβ1-3Galβ1-4Glc-PA 3 4 Fucα1 Fucα1	5.84	3.07
$3'\text{-Sulfo-}V^4Fuc\alpha,III^3Fuc\alpha\text{-}_{2,1}Lc_6$	HSO_3-3Galβ1-3GlcNAcβ1-3Galβ1-4GlcNAcβ1-3Galβ1-4Glc-PA 4 3 Fucα1 Fucα1	5.87	3.31
$3'\text{-Sulfo-}V^4Fuc\alpha,III^4Fuc\alpha\text{-}Lc_6$	HSO_3-3Galβ1-3GlcNAcβ1-3Galβ1-3GlcNAcβ1-3Galβ1-4Glc-PA 4 4 Fucα1 Fucα1	5.90	3.21

Table III. Elution positions in HPLC and mass analysis of neutral and acidic PA-oligosaccharides obtained from colon cancer cells of case 1 and unmatched to the accumulated standard oligosaccharides

Fraction	Elution position in HPLC Size (Gu)	RP (Gu)	Mass (observed)	Mass (calculated)	Estimated composition
N10-2	5.13	3.58	1151.4	1151.4 $[M+H]^+$	$Hex_4HexNAc_2$-PA
N12-2	5.66	3.78	1297.4	1297.5 $[M+H]^+$	$Hex_4HexNAc_2dHex_1$-PA
N13-1	6.03	2.96	1297.4	1297.5 $[M+H]^+$	$Hex_4HexNAc_2dHex_1$-PA
N13-2	6.02	4.31	1500.4	1500.6 $[M+H]^+$	$Hex_4HexNAc_3dHex_1$-PA
A5	3.63	4.83	1069.0	1069.4 $[M+H]^+$	HSO_3-$Hex_3HexNAc_2$-PA
A6	3.76	2.55	1012.0	1012.3 $[M+H]^+$	HSO_3-$Hex_3HexNAc_1dHex_1$-PA
A10-1	4.51	4.89	1231.1	1231.4 $[M+H]^+$	HSO_3-$Hex_4HexNAc_2$-PA
A10-2	4.52	5.54	1368.8	1368.5 $[M+H]^+$	$NeuAc_2Hex_3HexNAc_1$-PA
A13-1	5.05	5.15	1515.0	1514.6 $[M+H]^+$	$NeuAc_2Hex_3HexNAc_1dHex_1$-PA
A13-2	5.05	7.77	1522.2	1522.5 $[M+H]^+$	HSO_3-$NeuAc_1Hex_4HexNAc_2$-PA
A14	5.21	4.37	1377.2	1377.5 $[M+H]^+$	HSO_3-$Hex_4HexNAc_2dHex_1$-PA
A15	5.32	3.62	1377.1	1377.5 $[M+H]^+$	HSO_3-$Hex_4HexNAc_2dHex_1$-PA
A16-2	5.47	8.04	1668.2	1668.6 $[M+H]^+$	HSO_3-$NeuAc_1Hex_4HexNAc_2dHex_1$-PA
A17	5.62	4.82	1668.2	1668.6 $[M+H]^+$	HSO_3-$NeuAc_1Hex_4HexNAc_2dHex_1$-PA
A18	5.77	5.45	1442.3	1442.5 $[M+H]^+$	$NeuAc_1Hex_4HexNAc_2$-PA
A19	5.85	5.67	1668.0	1668.6 $[M+H]^+$	HSO_3-$NeuAc_1Hex_4HexNAc_2dHex_1$-PA
A20	6.04	3.01	1523.0	1523.5 $[M+H]^+$	HSO_3-$Hex_4HexNAc_2dHex_2$-PA
A21	6.31	5.56	1814.0	1814.6 $[M+H]^+$	HSO_3-$NeuAc_1Hex_4HexNAc_2dHex_2$-PA

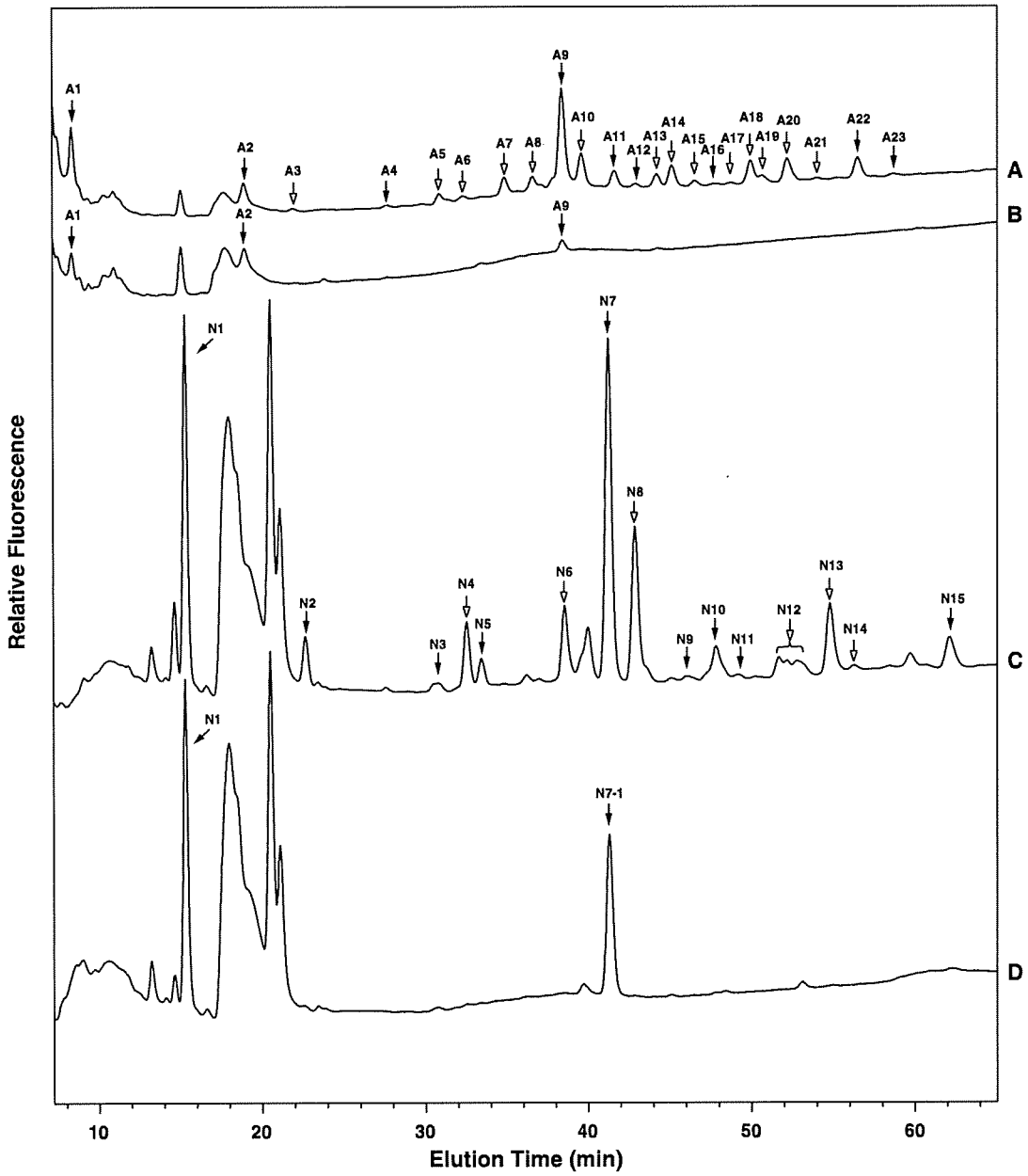

Fig. 1. Size fractionation HPLC of acidic and neutral PA-oligosaccharide mixtures obtained from CCs and NCs from case 1. A, acidic fraction of CCs, B, acidic fraction of NCs, C, neutral fraction of CCs, D, neutral fraction of NCs. Twenty-three and 15 major peaks found in acidic and neutral fractions of CCs are represented as A1-A23 and N1-N15, respectively, and highlighted with arrows (A and C). Three and two major peaks found in acidic and neutral fractions from NCs are numbered as per the peak numbers of CCs (B and D). Peaks shown with closed arrows and open arrows represent those usually and rarely observed in CCs from the other cases. Peaks at around 20 min in 1C and 1D are artifacts and not PA-oligosaccharides, as confirmed by mass spectrometry analysis.

Galβ1-3GlcNAcβ1-3Galβ1-4Glc-PA on the map, indicating the structure of the backbone to be Galβ1-3GlcNAc-Galβ1-3GlcNAcβ1-3Galβ1-4Glc-PA. Hydrolysis of N10-2 with endo-β-galactosidase gave two peaks by HPLC, corresponding to Glc-PA and GlcNAcβ1-3Galβ1-4Glc-PA. These results indicate that the subterminal GlcNAc is linked β1-3 to galactose. Hence, the structure of N10-2 is predicted to be Galβ1-3GlcNAcβ1-3Galβ1-3GlcNAcβ1-3Galβ1-4Glc (Lc_6). The structures of N12-2 and N13-2 were estimated to be VI^2Fucα-Lc_6 and VI^3GalNAcαVI^2Fucα-Lc_6, respectively, since the digestion product of N12-2 with α1,2-fucosidase and sequential digestion product of N13-2 with α-*N*-acetylgalactosaminidase, and then α1,2-fucosidase gave products which ran at the same position as Lc_6, as was determined in the above experiment.

Structure of N13-1 and A18

After sequential digestion with α1,3/4-fucosidase, β1,4-galactosidase, and β-*N*-acetylhexosaminidase, the digestion products of N13-1 ran on the 2D map at the same position as reference compound Lc_4. Under the conditions used in this study, α1,3/4-fucosidase can cleave a fucosyl residue linked to a subterminal fifth GlcNAc, but not an internal third

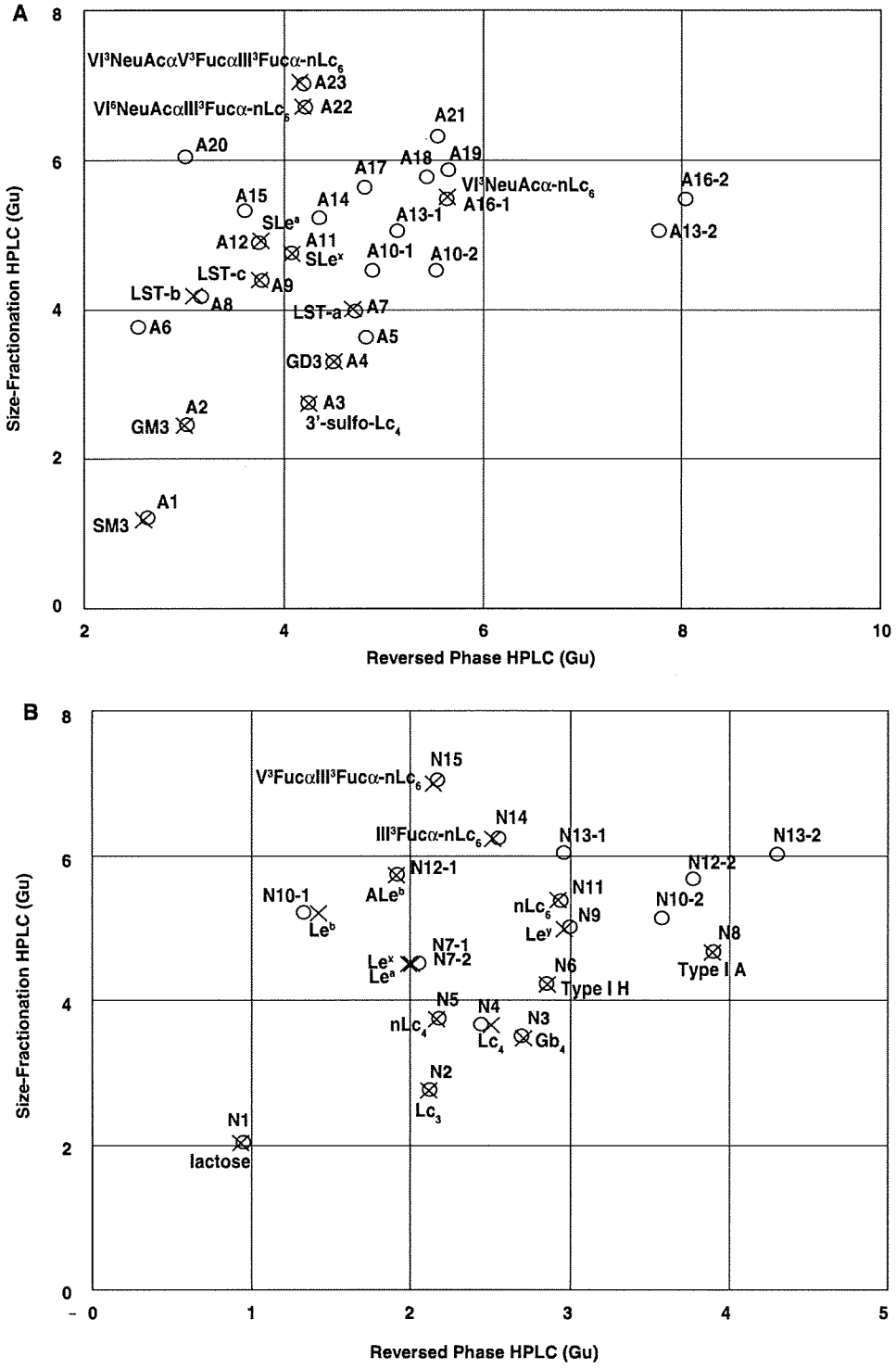

Fig. 2. Two-dimensional map of acidic and neutral PA-oligosaccharides obtained from CCs of case 1. (**A**) Acidic PA-oligosaccharides, and (**B**) neutral PA-oligosaccharides. The elution positions of each PA-oligosaccharide on the size-fractionation and reversed-phase HPLC are expressed in glucose units (Gu) based on the elution times of PA-isomaltooligosaccharides and plotted on the map. Circles indicate the positions of the acidic or neutral PA-oligosaccharides from CCs. X indicates the positions of the standard PA-oligosaccharides.